Master's thesis

NTNU
Norwegian University of Science and Technology
Faculty of Engineering
Department of Marine Technology

Gustav Svensson

Fatigue prediction models of Dynamic Power Cables by laboratory testing and FE analysis

Master's thesis in Nordic Master in Maritime Engineering
Supervisor: Svein Saevik, Jonas Ringsberg
June 2020

NTNU
Norwegian University of
Science and Technology

NTNU
Norwegian University of Science and Technology

CHALMERS
UNIVERSITY OF TECHNOLOGY

Fatigue prediction models of Dynamic Power Cables by laboratory testing and FE analysis

By

Gustav Svensson

Master's thesis in Maritime Engineering

Submission: 10th June 2020.
Supervisors: Prof. Svein Saevik, Prof. Jonas Ringsberg.

Department of Marine Technology
Facility of Engineering
Norwegian University of Science and Technology

Department of Mechanics and Maritime Sciences.
Division of Marine Technology
Chalmers University of Technology

NTNU Trondheim
Norwegian University of Science and Technology *Faculty of Engineering*
Department of Marine Technology

MASTER THESIS SPRING 2020

for

Stud. Tech. Gustav Svensson

Fatigue prediction models of Dynamic Power Cables by laboratory testing and FE analysis

Utmattingsmodeller for kraftkabler basert på kombinert testing og elementanalyse

Power cables used as dynamic risers connecting floating offshore wind turbines to the seabed infrastructure will be exposed to loads related to current, waves and associated floater motion. Full scale fatigue tests of copper conductors have been performed and are still ongoing. Meanwhile, small scale fatigue tests of each wire of the conductor have also been performed.
The master thesis work is to be carried out as a continuation of the project work performed during Fall 2019 where the major objective is to combine small scale test fatigue data with FE analysis to investigate the correlation with full scale test results. The work is to be carried out as follows:

1. Continue literature review into power cables, fatigue of copper conductors, relevant rules and standards, methods for structural analysis of cabled structures.
2. Establish models of the full-scale test set-up at different curvature radii and perform FE stress analyses.
3. Perform stress sensitivity analyses with respect to element mesh, contact stiffness by considering axial stiffness test data, modelling procedure and friction coefficient.
4. Perform fatigue analysis and compare to full scale test data.
5. Conclusions and recommendations for further work

The work scope may prove to be larger than initially anticipated. Subject to approval from the supervisors, topics may be deleted from the list above or reduced in extent.

In the report, the candidate shall present her personal contribution to the resolution of problems within the scope of the thesis work

Theories and conclusions should be based on mathematical derivations and/or logic reasoning identifying the various steps in the deduction.

The candidate should utilise the existing possibilities for obtaining relevant literature.

Thesis report format
The report should be organised in a rational manner to give a clear exposition of results, assessments, and conclusions. The text should be brief and to the point, with a clear language. Telegraphic language should be avoided.

The report shall contain the following elements: A text defining the scope, preface, list of contents, summary, main body of thesis, conclusions with recommendations for further work, list of symbols and acronyms, references and (optional) appendices. All figures, tables and equations shall be numerated.

The supervisors may require that the candidate, in an early stage of the work, presents a written plan for the completion of the work.

The original contribution of the candidate and material taken from other sources shall be clearly defined. Work from other sources shall be properly referenced using an acknowledged referencing system.

The report shall be submitted in electronic format (.pdf):
- Signed by the candidate
- The text defining the scope shall be included (this document)
- Drawings and/or computer models that are not suited to be part of the report in terms of appendices shall be provided on separate (.zip) files.

Ownership
NTNU has according to the present rules the ownership of the thesis reports. Any use of the report has to be approved by NTNU (or external partner when this applies). The department has the right to use the report as if the work was carried out by a NTNU employee, if nothing else has been agreed in advance.

Thesis supervisors:

Prof. Svein Sævik, NTNU, Dr. Naiquan Ye, SINTEF Ocean and Prof. Jonas Ringsberg, Chalmers.

Deadline: 10th of June, 2020

Trondheim, January 7, 2020

Svein Sævik

Candidate – date and signature: 9 June Gustav Svensson

Table of contents:

Preface

This master thesis presents the final work of the Joint Nordic Master's degree programme in Maritime Engineering with specialisation in offshore structures. The Joint programme takes place on two universities and the student receives one MSc diploma from each university. The work has been conducted at the Norwegian University of Science and Engineering during the spring semester of 2020. The scope of the work was suggested by Professor Svein Saevik who is also the main supervisor of this work. The work builds on a project work course (7.5 ECTS) conducted in the Autumn semester of 2019.

This work was written during the outbreak and under the restrictions of the Covid-19 pandemic. This forced me to work from home and to spend most of the days in a small student apartment, something that indeed affected my spirit and motivation. I am grateful for the relative mild restrictions in Norway. Being allowed to go running and clear my mind in the beautiful nature, now seems like a key factor for dealing with this time.

During the modelling phase, quite a lot of results had to be scrapped, this was quite stressful since one simulation takes roughly two weeks. The reason for this is mistakes done by me, but as well due to some bugs that were found in the software. Unfortunately, this delayed my work but since the bugs were fixed, a side effect of this work is an improved software.

Gustav Svensson

Acknowledgement

This master thesis is written for two universities, but the work has been carried out at Norwegian University of Science and Technology under the supervision of Professor Svein Saevik. His guidance, support, advice and time during this work are gratefully acknowledged. My secondary supervisor Professor Jonas Ringsberg at Chalmers is also acknowledged for his help and support.

I would also like to express my gratitude for all the support and love from my family and friends.

Abstract

Floating wind turbines are becoming more popular and is likely to be a major source of energy in the future. These floating turbines relies on dynamic subsea power cables for the transportation of electricity which are exposed to fatigue loading. It is desirable to be able to model these power cable for e.g. lifetime predictions. This work focusses on the conductor in the power cable. A FEM model was developed, and reversed bending was simulated. The results were compared to laboratory tests of the same kind and shows that the model overestimates fatigue life. This suggest that the fatigue damage process might be induced by fretting. The study also discusses the influence of mean stress effect and whether fretting is likely to occur based on a simplistic analysis.

Summary

In these days there are an increasing demand for carbon dioxide free energy. Many countries and EU have set goals to reach a carbon dioxide free energy supply in the near future. Wind power is one technique that plays an important role in reaching these goals. In the past, wind turbines have been built mostly onshore and to some extent offshore but in shallow waters. Because suitable land area is limited and increasing public complains, it is desirable to build further away from the shore and therefore in regions of deeper water. This also comes with the benefit of increased efficiency because wind speed tends to increase with distance from shore.

Floating wind turbines are a relatively new technique that allows the constructions to move into regions of deeper waters. Previously, offshore wind turbines have been built on fixed foundations which are limited to depths of 50-60 meters. Floating turbines thereby takes wind power into a new phase of its development because they can be installed at greater depths.

These floating turbines relies on dynamic subsea power cables for the transport of electricity from the turbine to the seabed. These cables are exposed to dynamic loads such as tides, waves and movement of the floating turbine, the fatigue life of the power cable must therefore be considered with regards to these loads.

Dynamic power cables have a complex mechanical behaviour involving several parts. This master thesis work focused on a conductor which is the part of the power cable that carries the electricity. A dynamic power cable needs to be flexible. This property comes from the mechanical behaviour of stick and slip domains. Initially, with none and little bending the cable behaves as a rigid beam. But as bending continues, sliding occurs between the layers in the cable which gives the cable its flexibility.

BFLEX FE software developed by Sintef was employed for modelling and simulation of the conductor. The conductor was simulated in tension-bending mode where it was bent over a bellmouth with two different radii of curvature. The intention was to represent the loading of a conductor hanging from a floater trough a bend stiffener (bellmouth) and exposed to the loads from motions of the floating turbine. The model was developed with the basis that fatigue life is mainly governed by longitudinal stress ranges. The fatigue life estimation was based on stresses from the model and SN-data from individual wires.

The result shows that when comparing to laboratory tests of the same setup, that the model overestimates fatigue life. This suggest that something more is going on and that

the fatigue life is not mainly governed by longitudinal stress ranges, in this test setup. It is likely that the fatigue damage process is induced by fretting. A simplistic fretting analysis was done based on displacement amplitude and contact pressure. This analysis shows that the conditions for fretting fatigue are sufficient to reduce the fatigue life. This is more likely to occur in the larger radius model which fits well with assumptions and the predicted life of the two models.

The study also shows that the friction coefficient and the shear stiffness of the contact elements has a strong influence on the result. Stresses due to friction comes from contact between the layers and hoop contact within the layer. It was found that the friction forces from the hoop contacts are small compare to inter layer contacts. This validates the analytical model which assumes no friction forces from hoop contact.

It is suggested for future work to further study whether fretting is present and also investigate the effect mean stress has on copper conductors.

List of figures

List of tables

Nomenclature

FEA	Finite element analysis
SCF	Stress concentration factor
DFF	Design fatigue factor
FEM	Finite element method
TL	Total Lagrange
UL	Updated Lagrange
MSC	Mean stress correction
$\bar{T}$	Mean global tension
$\bar{M}_T$	Mean global moment
ΔT	Dynamic tensile load
ΔM_T	Dynamic torque
$\Delta\beta$	Dynamic curvature
$\bar{F}_x$	Mean axial force
ΔF_x	Dynamic axial force in wire
ΔM_x	Dynamic torque moment around the helix tangential x-direction.
ΔM_y	Dynamic bending moment around the bi-normal y-direction.
ΔM_z	Dynamic bending moment around the surface normal z-direction
μ	Friction coefficient
α	Lay angle
θ	Angle trellis contact is formed at
M	Bending moment
E	Elastic modulus
I	Area moment of inertia
κ	Curvature
Q_1	Axial force in a single wire before slip.
A	Area
R	Radius of a layer
ψ	Polar coordinate of a cross-section
X^1	Local length coordinate along the helix
τ	Shear force
σ	Stress
$\Delta\sigma$	Stress range
σ_m	Mean stress
σ_a	Stress amplitude
R	Stress ratio (R-ratio)
σ_U	Ultimate strength
σ_y	Yield strength
N	Number of cycles until failure
m	Exponent in crack grow relation in the Basquin equation.
C	Constant in the Basquin equation
D	Damage
$\Delta\sigma_T$	Stress range from dynamic tension
$\Delta\sigma_{tc}$	Stress range from transverse curvature
$\Delta\sigma_{nc}$	Stress range from normal curvature
$\Delta\sigma_f$	Stress range from friction

EA_{full}	Axial stiffness of the conductor
$\Delta\kappa$	Curvature range
ε_c	Strain caused by mean static tension
p	Normal pressure
Q	Tangential force
a	Semi width of contact zone
P	Normal force
$\boldsymbol{S}$	Generalized modal point forces
$\boldsymbol{k}$	Element stiffness matrix
$\boldsymbol{v}$	Nodal point displacements
$\boldsymbol{S^0}$	Equivalent nodal point forces due to element loads.
$\boldsymbol{R}$	System nodal point forces of the structure
$\boldsymbol{K}$	System stiffness matrix
$\boldsymbol{r}$	Global displacement vector
$\boldsymbol{R^0}$	System equivalent nodal point forces due to element loads
ρ	Material density
$\ddot{\boldsymbol{u}}$	Acceleration field
$\boldsymbol{f}$	Volume force vector
$\boldsymbol{\sigma}$	Cauchy stress tensor
$\boldsymbol{\varepsilon}$	Natural strain
$\boldsymbol{t}$	Surface traction
$\boldsymbol{u}$	Displacement vector
$\boldsymbol{M}$	Global mass matrix
$\boldsymbol{C}$	Global damping matrix
$\boldsymbol{Q}$	Global load vector
ν	Poisson's ratio
ε	Strain
γ	Shear strain
θ	Rotation
$u_{i,j}$	the differentiation of the displacement components u_i along X^i with respect to the curvilinear coordinate X^J.
ε_1	First order axial strain
ε_2	Centreline rotations about X^3 axis
ε_3	Centreline rotations about X^2 axis
ω_1	Centreline torsion
ω_2	Curvature about X^2 axis
ω_3	Curvature about X^3 axis
ω_{ip}	The quantities represent the prescribed torsion and curvature quantities from bending.
κ_1	Initial total accumulated torsion of the cross-section centreline
κ_2	Initial accumulated curvature in the X^1- X^3 plane
κ_3	Initial accumulated curvature in the X^1- X^2 plane
κ_t	Transverse curvature

Cross-section

L1 = Core layer
L2 = First helical layer
T1 = First Tape layer
L3 = Second helical layer
T2 = Second tape layer
L4 = Third helical layer
T3 = Third tape layer

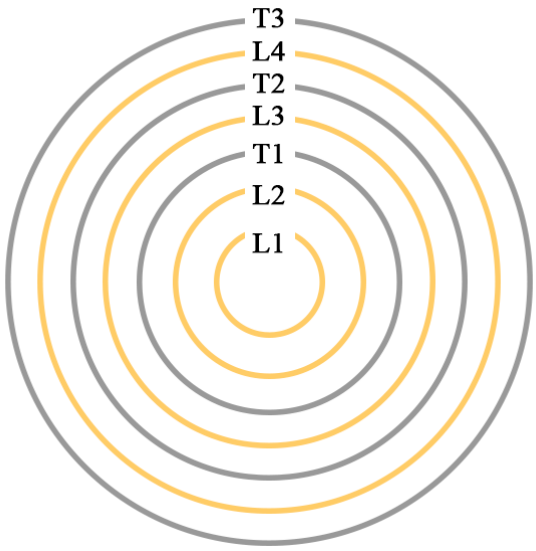

1. Introduction

This chapter presents a background, motivation and specifies the objectives of this master thesis. It also gives an introduction to some test data that is developed by others and used for comparison in this work.

1.1 Background

In these days there are an increasing demand for carbon dioxide free energy and wind power is one of the currently available techniques that meets this demand. Wind power is not a new technique, in fact, it has been an important source of energy to mankind throughout the history. The power of the wind was first used to power ships with the help of sails and later on wind was also used to pump water and to grind grains. Modern use of wind power uses turbines to convert mechanical energy into electrical energy.

Wind turbines are mostly built onshore but due to limited suitable land and public complaints about e.g. noise, the percentage of windfarms built offshore are increasing [1]. In the year of 2018, wind power was installed with a total capacity of 51.3 GW, were offshore installations correspond to about 8 percent or 4.5 GW. The offshore market is expected to continue grow in the near future, in the years of 2020-2023 a capacity of 4.9, 8.3, 9.9 and 10.1 GW is expected to be install, respectively [1].

Existing offshore wind turbines are mostly built on fixed seabed foundations, installations of this kind are restricted by a water depth of 50-60 meters. Many regions with the highest available energy have greater depths than this. Also, many coastal countries do not even have the opportunity to install offshore wind power with fixed foundations. The reason for this is the continental shelf, which drops away quickly and steeply, making the regions not suitable [2].

Floating wind turbines is a relatively new technique that allows installations to move into regions with deeper water. Another benefit that comes with this is that wind speed tends to increase with distance from shore. Some examples of different types of foundation structures are given in Figure 1.1. As floating wind turbines opens new markets and possibilities for a larger offshore energy capacity one might say that wind energy is entering a new phase of its development.

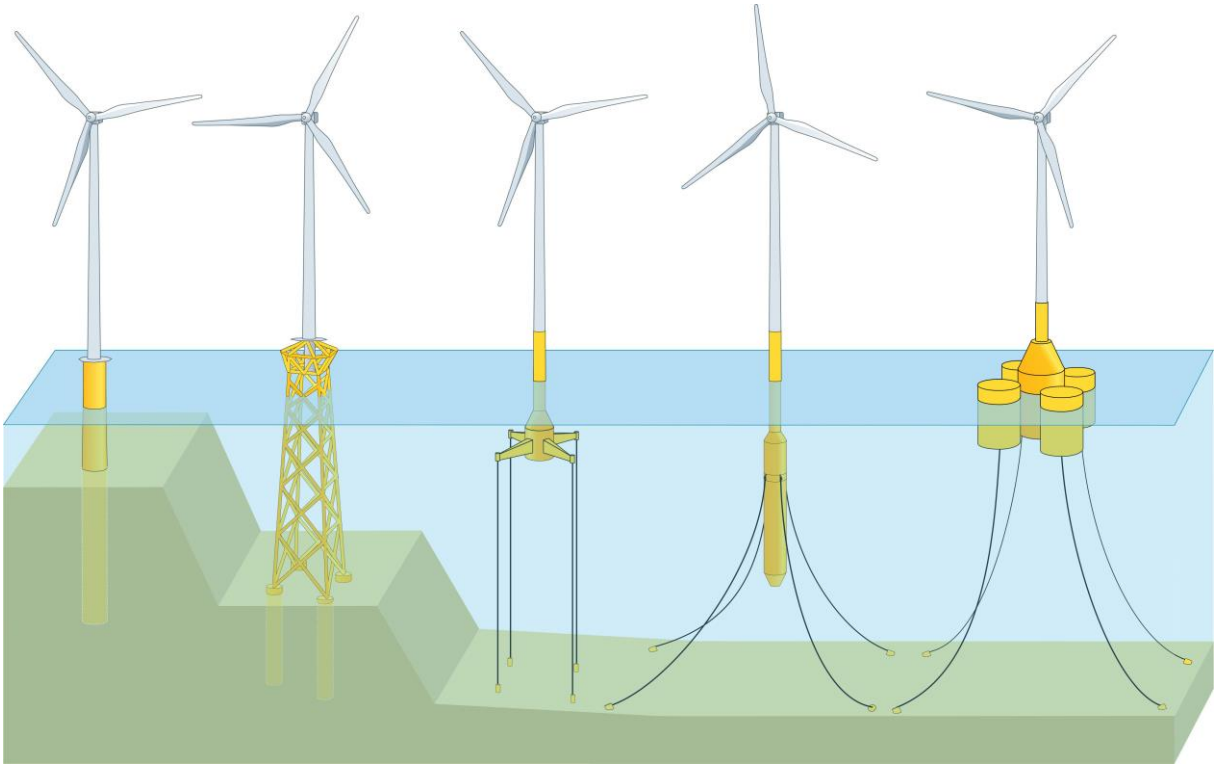

Figure 1.1: Different types of foundation structures [3].

As the demand for floating turbines increases so does it for subsea power cables. The power cable industry has experienced significant growth over the recent years and the demand is growing steadily. The grid network of a wind farm consist of different types of power cables which allows the electricity to flow from the turbines to the shore, an overview of a grid network is shown in Figure 1.2 [4].

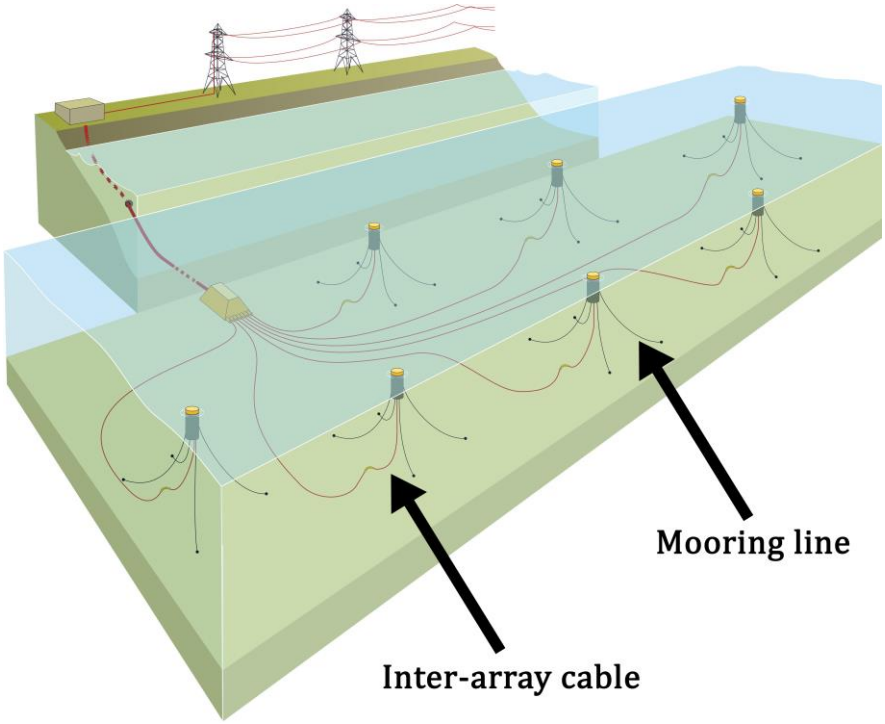

Figure 1.2: Grid network. Reproduced from [3].

The inter-array cable connects the floating turbine to the seabed. This cable, also referred to as a dynamic subsea power cable, is exposed to fatigue loading from waves, currents and from movements of the floating platform [4]. A typical dynamic power cable has voltage of 10-36 kV and consists of three copper conductors [5]. The cable can either hang freely from the platform down to the seabed or buoyant modules can be attached to the cable, a common configuration of such modules is what creates the "s-shape" shown in Figure 2.3. The purpose of distributing modules in this way is to minimize dynamic responses by decoupling the platform motion from the seabed connection point [4]. The turbines can also be connected between each other instead of to the seabed. This work represents the situation and loading of a conductor hanging from a floater trough a bend stiffener (bellmouth) being exposed to loads from motions of a floating turbine.

1.2 Motivation

Many countries and EU have set up goals to achieve a carbon dioxide free energy production in the near future. The trends seen today suggest that floating wind power will play an important role in reaching these goals. Therefore, it is of interest to use numerical models to predict stresses in power cables used for these applications.

The main goal of this master thesis is to combine small scale test fatigue data with FE analysis to investigate the correlation with full scale test results. This is done in order to reduce the gap between observed test data and finite element analysis.

1.3 Objectives

The main objectives of this master thesis are:

1. Continue literature review into power cables fatigue of copper conductors, relevant rules and standards, methods for structural analysis of cabled structures.

2. Establish models of the full-scale test set-up at different curvature radii and perform FE stress analyses.

3. Perform stress sensitivity analyses with respect to element mesh, contact stiffness by considering axial stiffness test data, modelling procedure and friction coefficient.

4. Perform fatigue analysis and compare to full scale test data.

5. Conclusions and recommendations for further work.

1.4 Laboratory test data

The results of this master thesis are based on and compared to experimental tests done by Nasution et al. [6, 7]. The fatigue life prediction is based on a SN-curve developed by single wire test data and the results of the model are compared to test data of the full cross-section conductor.

The single wire tests were done in tension-tension mode until failure. The full cross-section conductor tests were done in tension-bending mode in a test rig. The bending was applied in one plane and the procedure was monitored by extensive instrumentation. The failure criteria for the full cross-section tests was taken as when a rapid change of the conductor length was measured. The fracture was investigated with a scanning electron microscope and no signs of fretting was found. The results of the full cross-section tests are show in Table 1.

Table 1: Results of tension-bending test of the conductor

Radius of curvature [m]	No. of cycles to failure	Remark	Failure position (Layers)
3	212 644	Unlubricated	2^{nd} – 3^{rd}
3	225 244	Unlubricated	2^{nd} – 3^{rd}
3	262 394	Unlubricated	2^{nd} – 3^{rd}
6.5	617 474	Unlubricated	2^{nd} – 3^{rd}
6.5	951 059	Unlubricated	2^{nd} – 3^{rd}
6.5	980 782	Unlubricated	2^{nd} – 3^{rd}
3	387 178	Lubricated	2^{nd}
3	372 636	Lubricated	2^{nd}
3	434 643	Lubricated	2^{nd}

1.5 Limitations

The progress of this work resulted in a move towards theory of fretting and mean stress effect on copper. When studying these fields, one often faces material science such as microstructures, grain sizes etc. This has been noted but not studied in depth since it is beyond the scope of this work.

2. Subsea Power Cables

This chapter introduces subsea power cables. Several topics are covered in order to understand the mechanics and to design them.

2.1 General design of subsea power cables

Several different designs and configurations of power cables exists. Thies et al. [8, 9] describes the main 7 components that a typical subsea power cable consists of as:

- *Conductor core.* The core carries the electrical current and consists of several layers of wires.
- *Electrical insulation*. The conductor is insulated by the possible use of three different design/materials types: traditional oil-impregnated paper, cross-linked polyethylene or ethylene propylene rubber.
- *Screen.* A semiconducting layer around the core that reduces the electric field strength and avoids field concentration zones.
- *Sheath*. A metal layer around the core that acts as a water barrier and protects the cable against fault currents.
- *Armature.* An outer metal armature that provides the cable with mechanical strength and impact protection. Usually made of galvanized steel wires.
- *Optic fibre.* Optional, used for data transmission and monitoring.
- *Protecting sheath.* An outer layer that consists of polypropylene for abrasion resistance.

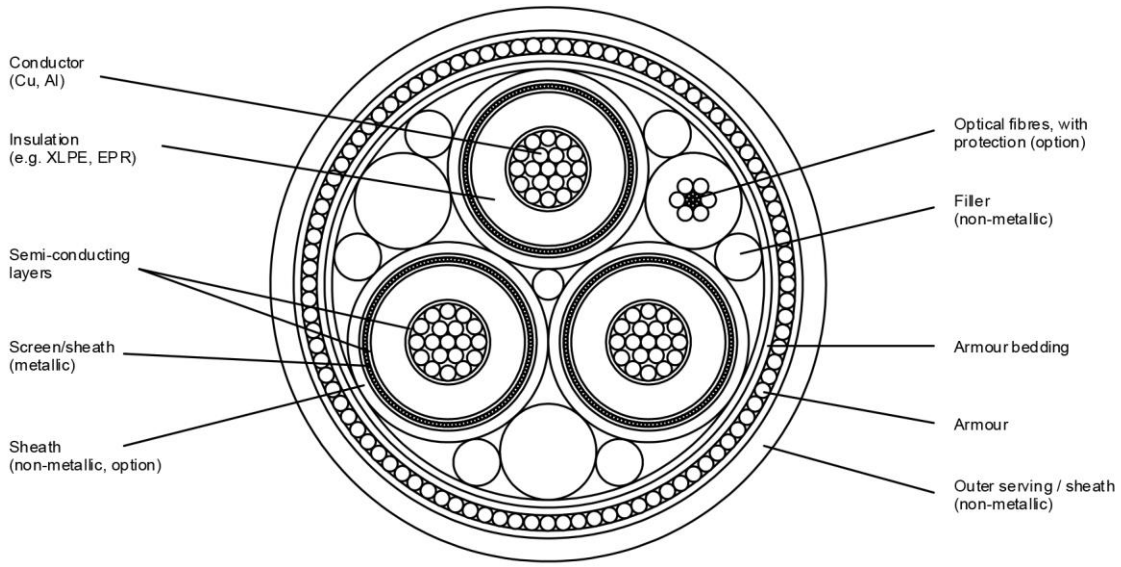

Figure 2.1: Typical three-core power cable [10].

The cable is designed by combining the components in a cylindrical and/or helical configuration and with different sizes. Cable design is commonly tailored by the manufacturer for a specific application and standardized cables does not exist [9]. A typical subsea power cable is shown in Figure 2.1.

The vast majority of existing subsea power cables are used in static applications. This means that they are connected to a fixed structure and not exposed to any significant fatigue loading. Floating wind turbines requires cables that are not fixed and thus exposed to fatigue loading. Static cables are too vulnerable for fatigue loads and therefore are dynamic power cables required for these load applications [9].

2.2 Conductors

The main purpose of a power cable is to transport electricity and the conductor(s) is the responsible component for this. Conductors are usually made of copper or aluminium. The choice of material depends on price and application. Copper is more expensive than aluminium. However, power cables with copper conductors are less expensive since copper allows a smaller cross-section of the conductor and thus are less lead and steel needed for the outer layers [5]. Some example of data for typical conductors for subsea power cables are given in Table 2.

Table 2: Example of typical conductors for subsea applications [4]

Nominal cross-section area of copper conductor [mm]	95	120	185	240
Outer diameter [mm]	104	106	114	119
Weight [kg/m]	16	18	21	23

Conductors can be designed in many ways and some common designs are shown in Figure 2.2. Conductors in subsea power cables are mostly stranded from round wires. In the manufacturing process of these, single wires are laid up in layers and placed in a stranding machine. The conductor is then compressed either layer by layer or at the end of the stranding machine. The compression is done by dies or roller sets and reduces the gaps between the wires of the conductor. A filling factor of 92 percent is achievable for round wires [5].

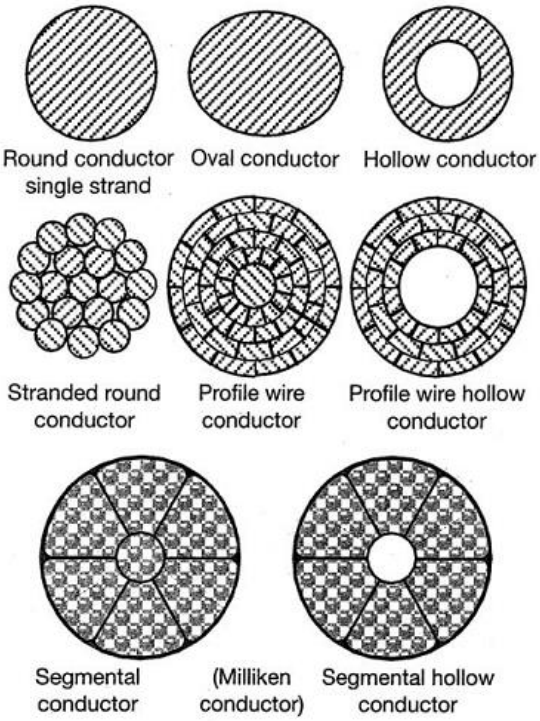

Figure 2.2: Different conductor designs [5]

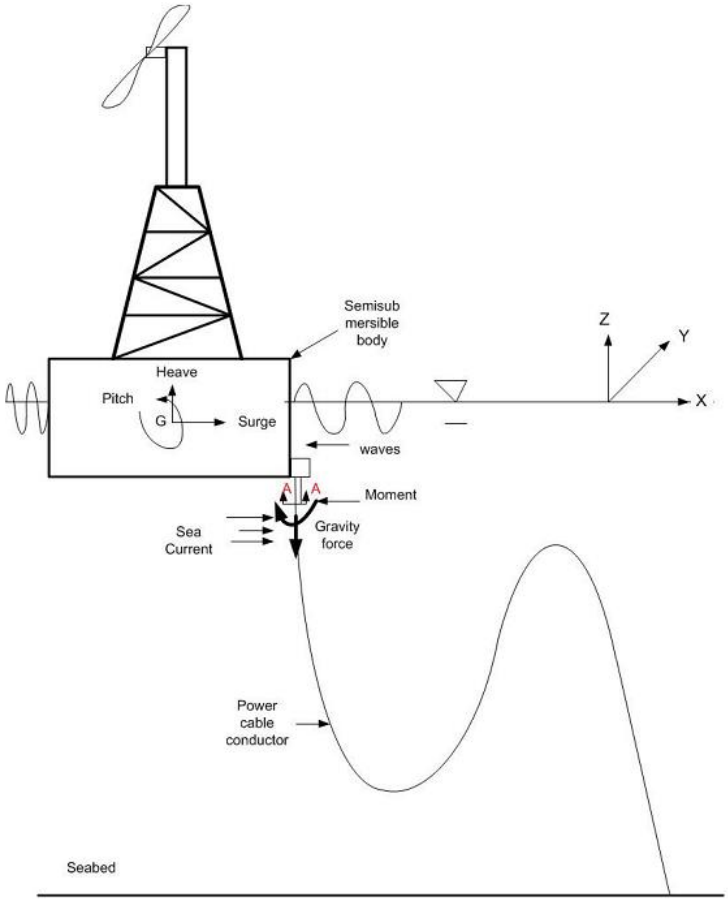

Figure 2.3: Motions on a power cable [7].

2.3 Terminology

The terminology in this section is taken from Nasution et al. [7] and shown in Figure 2.4.

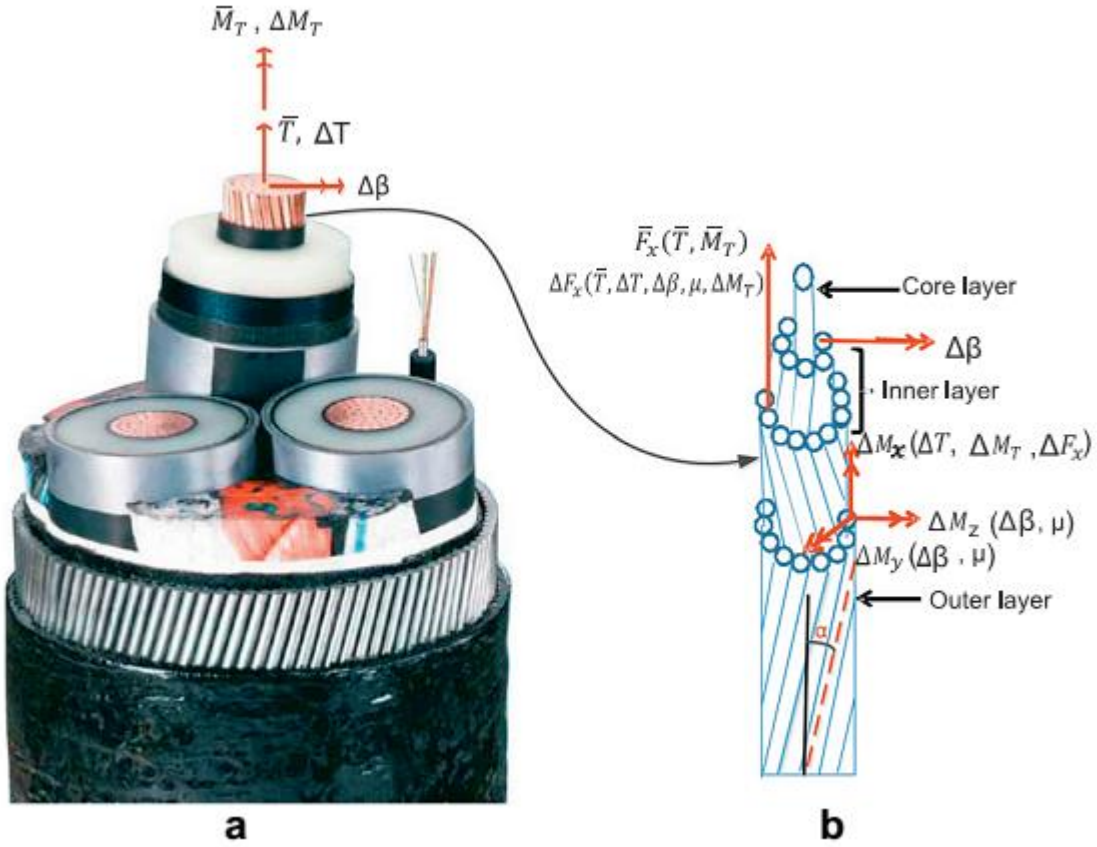

Figure 2.4: Forces on a conductor [7].

The power cable is exposed to several forces such as gravity, waves, and movement of the connecting point. Gravity causes:

- A mean global tension, $\bar{T}$.
- A mean global moment, $\bar{M}_T$.

Heave and surge motion of the connection point causes:

- A dynamic tensile load, ΔT.
- A dynamic torque, ΔM_T.

Pitch and roll motions cause dynamic curvatures, $\Delta\beta$, acting on the conductor. The most heavily loaded section of the conductor is close to the connection point. Each individual wire is subjected to a mean axial force, $\bar{F}_x$, which is a function of the mean global tension and the mean global moment. Each wire is also subjected to a dynamic axial force, ΔF_x, which is a function of dynamic tensile load and torque, dynamic curvatures and the coefficient of friction, μ, between the layers. The dynamic curvature causes local bendings in each wire:

- ΔM_x, a dynamic torque moment around the helix tangential x-direction.
- ΔM_y, a dynamic bending moment around the bi-normal y-direction.
- $\Delta M_{y,}$ a dynamic bending moment around the surface normal z-direction.

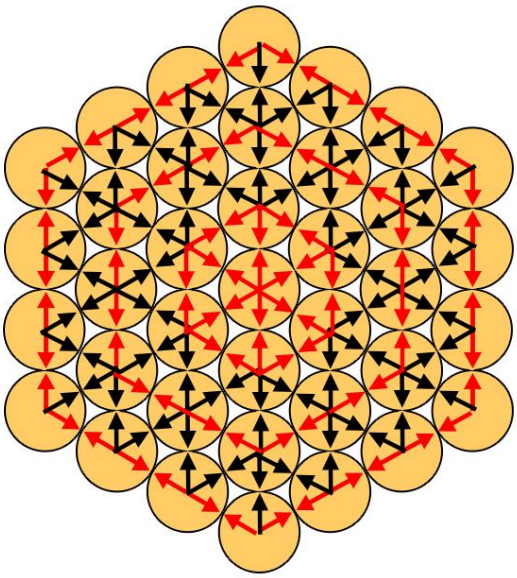

Figure 2.5: Cross section of conductor including contact forces. Red arrows show inline contact and black arrows show point (trellis) contact.

A typical stranded round conductor consists of several wires that are stranded helically into layers, as shown in Figure 2.4 b. This stranding leads to both inline- and point (trellis) contact. Inline (hoop) contact occurs between the core layer and the first helical layer, and within the helical layers. Point (trellis) contact occurs between two helical layers. Figure 2.5 illustrates inline and trellis contact on a conductor cross-section. The global axial force causes longitudinal and transverse forces in each layer of the conductor, the transverse forces causes a reduction of the conductor diameter.

If wires are pressed together, they deform, and a small contact area occur at the trellis point as illustrated in Figure 2.6 B. The trellis contact is formed at an angle θ given by the lay angle α. This is a result of the manufacturing of the conductor.

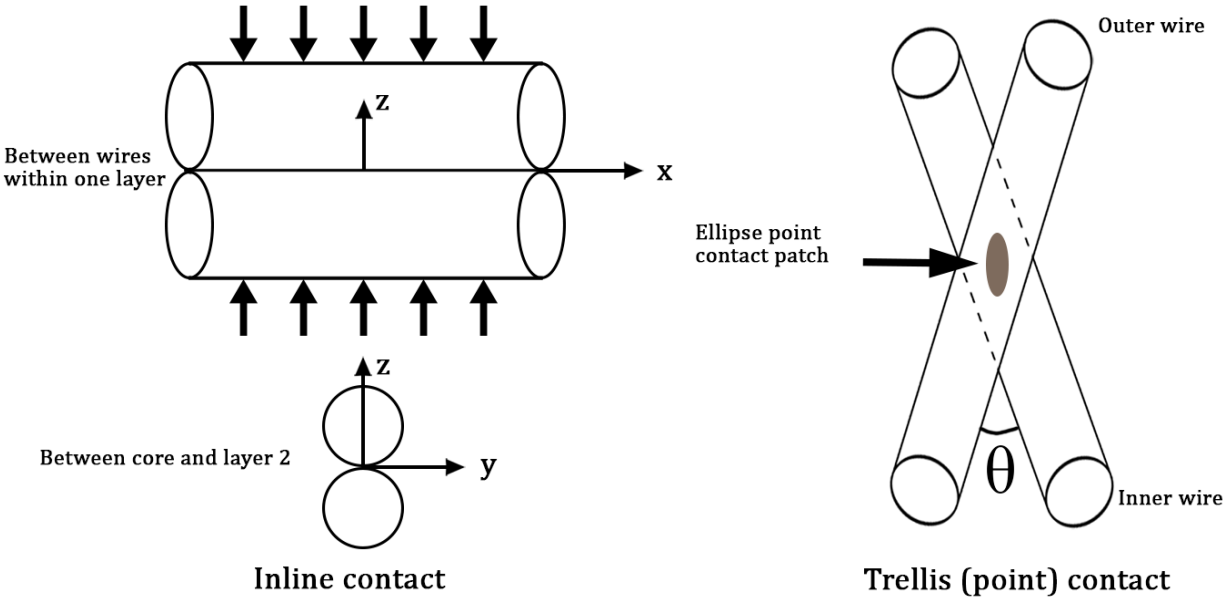

Figure 2.6: Inline and trellis contact.

2.4 Fatigue of copper conductors

A literature research of fatigue and contact stresses of cabled structures was conducted in the prior project work to this master thesis. The following section is based on that research but have been customized and continued for this work. Cable structures includes ropes and strands. The main difference between a rope and a strand is that individual wires in a strand follows a simple helical path, while as wires in a rope follows a more complex helical path in strands, where the strands themselves are formed into helices. In this work is the considered conductor designed like a strand.

Johnson [11] described the Hertz contact stresses due to a normal load occurring between two solid bodies. A contact theory was developed, predicting the geometry of the contact area and how the size changes with increasing load. The theory also predicts magnitude and distribution of surface tractions and more.

Hobbs and Ghavami [12] investigated fatigue of socketed structural wire strands. They concluded that failure behaviour was governed by different failure mechanisms related to the contacts conditions near the socket.

Alani and Raoof [13] investigated the effect of mean axial load on axial fatigue life of spiral strands. They found that due to the wire flattening at the trellis points of the interlayer contacts, the fatigue life increases with increasing levels of mean stress for a given lay angle. They also concluded that fatigue life decreases with increasing lay angle

The fatigue life of a multilayer stranded steel wire or rope is considered to be governed mainly by fretting fatigue, which is due to stress concentration in the trellis contact point [14, 15] . Hobbs and Raoof [14] further reports that lubrication is an important factor in fatigue strength. They also suggest that due to the complexity of fretting fatigue

in stranded objects, fatigue tests should be representative of the actual inter-wire movements in the cable. This means that whole cables should be tested.

Raoof [16] used single wire data to develop a theoretical model that, for a constant load amplitude, predicts axial fatigue of the full cross-section. The model correlates well with experimental data. Raoof [17] concluded that the model provides upper bounds for the fatigue life of cables that fails at the end termination, and also that the observed fatigue life is significantly affected by the termination type.

A model for predicting fretting fatigue due to inter-wire contact stress was introduced by Hobbs and Raoof [18]. The model considers inline and trellis contact stresses, also frictional effects were considered. Both tension and bending load cases are included in the model.

Copper conductors in power cables are surrounded by an outer armour of steel wires and bend stiffeners, this reduces forces and curvatures in the conductor. Stranded conductors are similar to stranded steel wires in design, however, the materials copper and steel behaves differently. This master thesis focuses on copper conductors and the rest of this section is dedicated to literature research concerning them.

Karlsen [19] investigated fatigue of copper conductors for dynamic subsea power cables. A test method for simulating strain range fatigue was presented, including effects from friction, fretting, creep properties of copper and high tension at deep waters.

Nasution et al. [7] investigated fatigue performance by experimental tests and by finite element analysis (FEA) of a 95 mm^2 copper conductor. The experimental tests were performed both on individual wires and on full cross-section conductors, FEA was performed on an individual wire. The individual wire tests were done in tension-tension loading and the full cross-section tests in tension-bending loading. The experiments showed that fatigue strength of full cross-section conductors is lower than for individual wires. The reason for this is cracks arising from the vulnerable trellis point. This point is a result of the manufacturing of the conductor and causes surface irregularities in the wire, as shown in Figure 2.7.

The same study also shown that fatigue strength of individual wires taken from the outer layer is less than wires taken from the inner layer, this is due to larger surface irregularities. Fractures were investigated with a scanning electron microscopy. This showed, for single wires, that fatigue initiation arises from cracks close to the thinnest section of the wire. For the full cross-section, all failures occurred in the inner layer and fractography showed fatigue initiation from the outside of the wire, at the trellis contact with the outer layer.

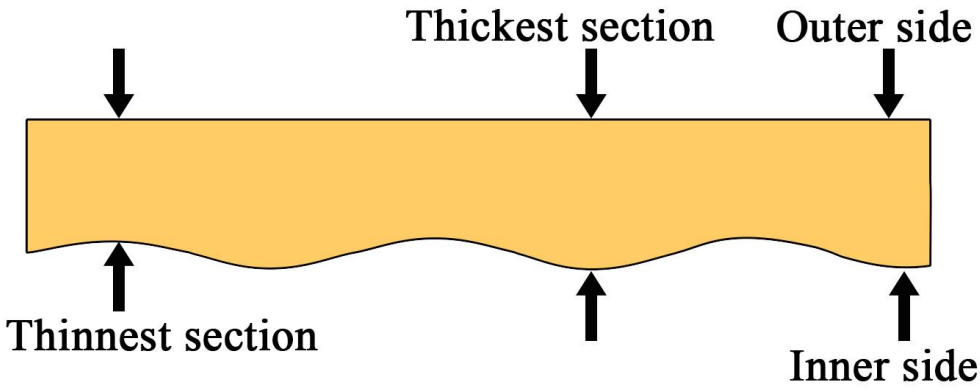

Figure 2.7: Surface irregularities of a wire [20].

A similar study was performed by Nasution et al. [21] investigating a 95 mm^2 full cross-section conductor in tension-tension and tension-bending modes with FEA. The models were based on beam and beam contact elements and concluded to be valid as long as longitudinal stresses governs fatigue performance. The FEA model predicts first failure in the outer layer for tension-tension and in the inner layer for tension-bending, all in accordance with experiments. The tension-tension tests indicate that fatigue failures were govern by local stress concentration factors (SCFs). The tension-bending tests indicate that the effect of friction between the layers plays an important role in fatigue life.

Nasution et al. [6] investigated fatigue strength of a 300 mm^2 copper conductor experimentally and by FEA. The study concludes that wires from 95 mm^2 and 300 mm^2 conductors tested in tension-tension loading falls in a common scatter band when maximum stress due to SCFs are considered. It supports previous conclusions that fatigue initiations arise from cracks at the trellis point. The study also showed that lubricated conductors have a longer fatigue life than unlubricated conductors. FEA based on fatigue strength of individual wires predicted that the second layer had the shortest fatigue life, full scale tests showed failures in either the second or third layer. Fatigue failure occurs in the inner layers because the contribution from friction forces is largest there. Also, in this study, an analytical method for calculating stress variation of individual wires of the conductor was developed.

2.5 Standards and Guidelines

In the progress of designing subsea power cables, different standards can be used as guidelines. Since applications of dynamic power cables are relatively new, there is a lack of standards for them. However, DNV-GL has two standards that can be used, DNV-GL-ST-0119 and GL-ST-0359. Certification of a cable design requires that these two standards are applied and that their requirements are fulfilled.

DNVGL-ST-0359 (subsea power cables for wind power plants) provides an overview of standards for subsea power cables. DNVGL-ST-0119 (floating wind turbine structures) has a section dedicated for power cables.

IEC 60228 is an international standard for conductors of insulated cables. It includes, among other things, requirements for numbers and sizes of wires. Solid and stranded conductors made out of both copper and aluminium is included. Also, fixed installations and dynamic applications are included. IEC 60502 concerns cables with extruded insulation.

2.6 Stick and Slip behaviour

The conductor consists of helical layers that are free to move and subjected to friction forces. Initially and for small curvatures, the shear force is less than the available friction force. In this state, the wires are restrained by the friction and the conductor behaves as a rigid body with constant bending stiffness. For this state, the plane surfaces remain plane assumptions holds true and the following relationship from standard beam theory between bending moment and curvature is valid.

$$M = EI\kappa \tag{2.1}$$

As the shear force increase it eventually overcomes the friction force and the wires starts to slip. This slip results in a decrease of bending stiffness, this is due to the movement of the wires, as they move, they cannot contribute to the bending stiffness as much as they could in the rigid body behaviour. It is due to the reduction of bending stiffness that the cable gets its desirable flexible properties.

It is known from standard beam theory that in bending, the shear stress distribution follows a parabola with maximum value at the neutral axis. Therefore, the slip process of the wires does not start at the same time. By considering a cross-section of the conductor, wires at the neutral axis starts to slip first and the wires with the greatest distance from the neutral axis will be last to slip. A conductor with three helical layers has therefore three critical curvatures values describing where the slip process starts for each layer.

At what curvature slip begins for a layer can be estimated analytically. The Axial force before slip in a single wire is given by:

$$Q_1 = EA\cos^2\alpha\, R\, \kappa \cos\Psi \tag{2.2}$$

where EA is the axial stiffness, α is the lay angle, κ is the curvature, R is the helix radius. With the relation for the circumferential coordinate:

$$\Psi = \frac{\sin\alpha}{R}\, X^1 \tag{2.3}$$

where X^1 is the local length coordinate along the helix. Differentiation of the axial force with respect to the local length coordinate gives the maximum shear force:

$$\frac{dQ_1}{dX^1} = EA\cos^2\alpha\,\kappa\,\sin\Psi\sin\alpha = \tau_{max} \tag{2.4}$$

The maximum shear force is found at the neutral axis and the following expression gives the critical curvature where slip begins:

$$\kappa_{cr} > \frac{\tau_{max}}{EA\cos^2\alpha\,\sin\alpha} \tag{2.5}$$

This means that until full slip is reached, one part of the cross section will be in stick and one part will be in slip as shown in Figure 2.8. Full slip is reached at a curvature with a factor of $\frac{\pi}{2}$ larger than the critical curvature where slip begins [22]. Because of the stick and slip effect, the relationship between stress and curvature results in a hysteresis loop that corresponds to the work done by the friction force at the contact interfaces after slip.

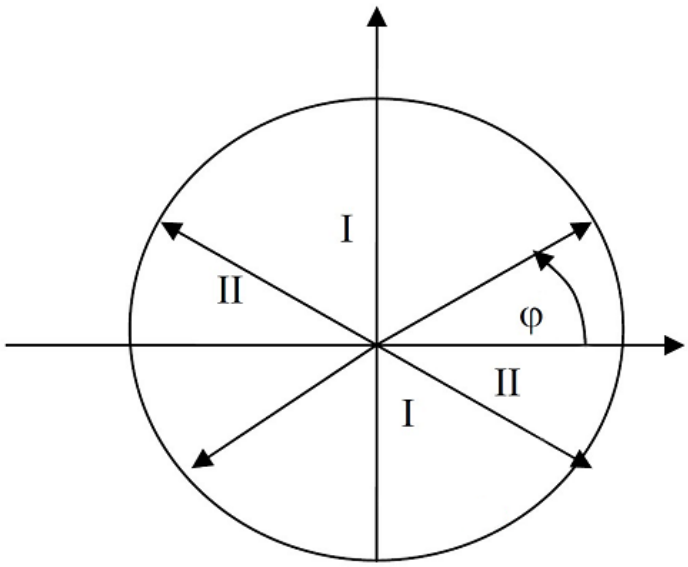

Figure 2.8: Stick (I) and Slip (II) zones of a cross-section. Reproduced from [23].

3. Fatigue

This chapter introduces the fatigue phenomenon of metallic structures. A general overview is given together with an analytical model specifically developed for calculating stress ranges in a copper conductor.

3.1 Introduction

Fatigue is a phenomenon that weakens a material and occurs when the material is exposed to repeated cyclic loading, usually with loads corresponding to stresses significantly lower than yield stress. The fatigue damage per cycle may be insignificant and not even detectable, however fatigue failure is a result of a cumulative damage process. The process contains the following three stages.

1. Crack initiation, N_i
2. Crack growth, N_g
3. Final failure

The total fatigue life, N, can be calculated by:

$$N = N_i + N_g \tag{3.1}$$

For a sinusoidal load variation as shown in Figure 3.1 some basic parameters are introduced to describe cyclic stress loading [24]:

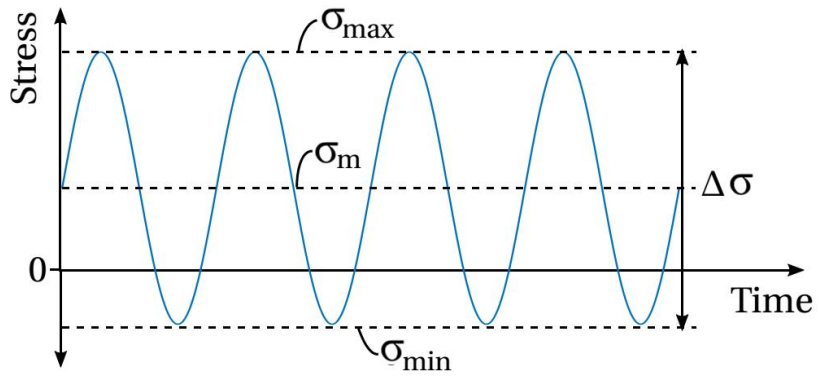

Figure 3.1: Stress ranges. Reproduced from [24]

σ_{max} is the maximum stress in a cycle, σ_{min} is the minimum stress in a cycle and $\sigma_m$is the mean stress in a cycle. The stress range is established from the figure as:

$$\Delta\sigma = \sigma_{max} - \sigma_{min} \tag{3.2}$$

The stress ratio (R-ratio) is defined as:

$$R = \frac{\sigma_{min}}{\sigma_{max}} \tag{3.3}$$

Fully reversed loading, zero-tension loading, and static loading corresponds to R-ratios of -1, 0 and 1, respectively. The stress range can be related to R-ratio by:

$$\Delta\sigma = 2\sigma_m \frac{1-R}{1+R} \tag{3.4}$$

Fatigue can be divided into low cycle fatigue (LCF) and high cycle fatigue (HCF). High cycle fatigue has a life of more than 10^5 cycles. Offshore structures are mainly in the high cycle range and this is also what is used in standards [24].

3.2 Mean stress correction

A mean stress value not equal to zero affects the fatigue life and must be considered. An increase of mean stress normally decreases the fatigue life. SN-curves (see next section) are used with stress amplitude but are produced with and depends on a certain level of mean stress. Constant life diagrams can represent the effect of mean stress. The two most common are the modified Goodman- and Gerber relation. Some experiments for steel have shown that the truth lies somewhere in this range depending on material where Goodman is the conservative. The relations are shown in Figure 3.2, known as a Haig's diagram and are given by:

Modified Goodman relation: $$\sigma_a = \sigma_a|_{\sigma_m=0}\left\{1 - \frac{\sigma_m}{\sigma_U}\right\} \tag{3.5}$$

Gerber relation: $$\sigma_a = \sigma_a|_{\sigma_m=0}\left\{1 - \left(\frac{\sigma_m}{\sigma_U}\right)^2\right\} \tag{3.6}$$

where σ_a is the stress amplitude for a nonzero mean stress, $\sigma_a|_{\sigma_m=0}$ is the stress amplitude for fully reversed loading i.e. when $\sigma_m = 0$, σ_y is the tensile stress and σ_U is the ultimate strength of the material [25].

It should be noted that this theory is based on steel and there are therefore uncertainties when applying this theory on copper. However, there are more methods that can be considered, see for e.g. Dowling [26]. Dowling also states that the sensitivity to mean stress seems to increase for higher strength metals. Mean stress effect that differs from

the traditional approach described above, is referred to as anomalous mean stress sensitivity (AMSS).

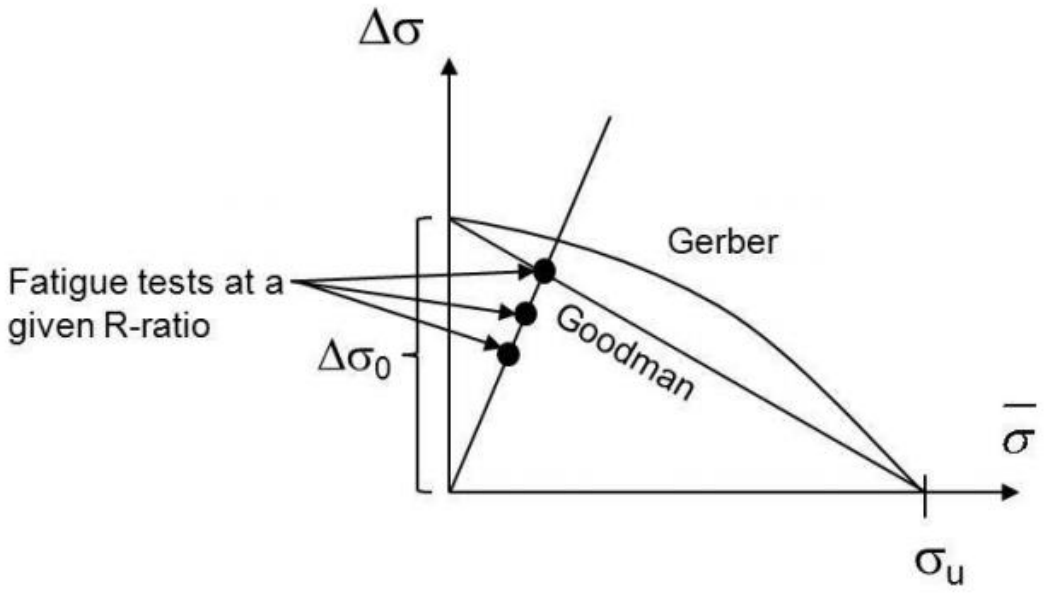

Figure 3.2: Haig's Diagram [23]

3.3 The SN-Approach (Whöler curves)

This approach is based on experimental data from fatigue tests. The stress-life diagram or SN-diagram shows how many stress cycles that a material can withstand for a given stress range. The fatigue life is only related to the stress range until a certain threshold, at lower range, the fatigue life may become infinite. The concept of infinite life only applies in a none-corrosive environment and where all the cycles are below the threshold. Also, this work is based on copper, which is generally considered not having a fatigue limit. The SN-curve is typically plotted on log-log format since fatigue life normally spans over a large number of cycles. A SN-curve is shown in Figure 3.3 and the mathematical relationship is given by:

$$N \cdot (\Delta\sigma)^m = C \tag{3.7}$$

where C is a constant, m is an exponent in crack growth relation and N is the number of cycles until failure [24]. The SN-curve has by definition a failure probability of 50 percent. Big margins are common in fatigue, in a design curve are often 2 standard deviations used as a safety margin, resulting in a 97.6 percent probability of survival.

Karlsen [19] points out that for copper conductors, it may be more suitable to use a strain-based approach. The reasons for this are the poor creep properties and nonlinear stress-strain relationship of the copper. However, in this work is a stress-based approach used for simplicity.

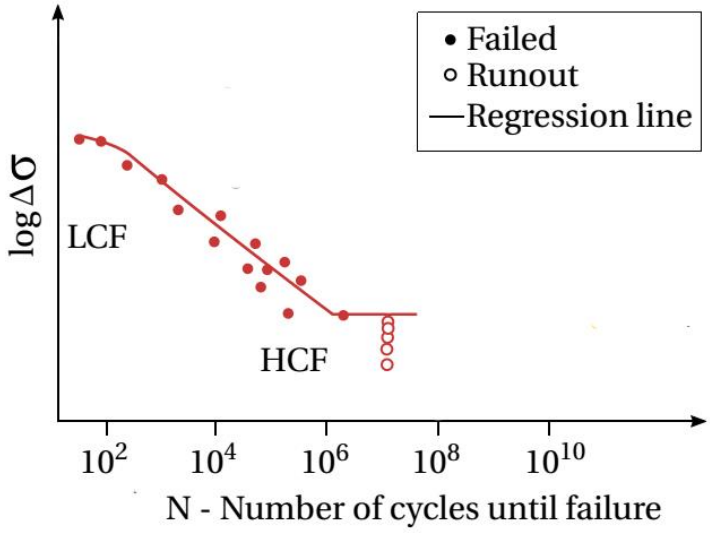

Figure 3.3: SN- Curve. Reproduced from [24].

3.4 Cumulative damage – Miner sum

SN-curves are based on data from stress ranges with constant amplitudes and are therefore only relevant for constant amplitude fatigue loading. In reality, structures are exposed to environments that causes irregular: amplitudes, mean stress levels and frequencies on the structures. E.g. loads from waves and tides on marine structures. The Miner-Palmgren cumulative damage rule is a simple approach that considers irregular loading. The rule assumes linear damage, this assumption should be taken with care since sequence and interaction of events may influence the fatigue life. For *i* number of different stress ranges the damage or Miner sum is given by:

$$D = \sum_i \frac{n_i}{N_i} \tag{3.8}$$

where n_i is the number of cycles for a constant stress range and N_i is the number of cycles that the given stress range can survive, fracture normally occurs once $D = 1$.

Cycle counting methods are often used to reduce the load history into series of constant stress amplitude. There are many methods on how to do this, general consensus is that the *Rainflow counting method* is the best. In standards a design fatigue factor (DFF) is used so that it satisfies:

$$D \cdot \text{DFF} \leq 1.0 \tag{3.9}$$

Different DFFs are recommended depending on safety class.

3.5 Analytical calculation of stress ranges

Nasutian et al. [21] developed an analytical model for calculating stress ranges of individual wires in a stranded conductor cross-section. The longitudinal stress range can be calculated by:

$$\Delta\sigma = \Delta\sigma_T + \Delta\sigma_{tc} + \Delta\sigma_{nc} + \Delta\sigma_f \tag{3.10}$$

where $\Delta\sigma_T$ is the stress ranges from dynamic tension, $\Delta\sigma_{tc}$ is the stress ranges from transverse curvature, $\Delta\sigma_{nc}$ is the stress ranges from normal curvature and $\Delta\sigma_f$ is the stress ranges from friction.

Stress ranges from dynamic tension

The axial stiffness of the conductor can be calculated by:

$$EA_{full} = EA\left(1 + \sum_{i=1}^{m} n_i \cos^3 \alpha_i\right) \tag{3.11}$$

where EA is the axial stiffness of each wire, n_i is the number of wires in helical layer i and α_i is the lay angle of layer i. Dynamic tension causes a stress variation in each wire according to:

$$\Delta\sigma_T^i = E \cos^2 \alpha_i \frac{\Delta T}{EA_{full}} \tag{3.12}$$

Elastic bending stresses

For the bending moment about the helix bi-normal axis, the corresponding stress range can be approximately determined for small lay angles by:

$$\Delta\sigma_{nc} = R_{nominal} E \cos^2 \alpha_i \cos 2\alpha_i \Delta\kappa \cos\Psi \approx R_{nominal} E \Delta\kappa \cos\Psi \tag{3.13}$$

where $\Delta\kappa$ is the curvature range and Ψ is the polar coordinate angle defining the helix position as shown in Figure 3.4.

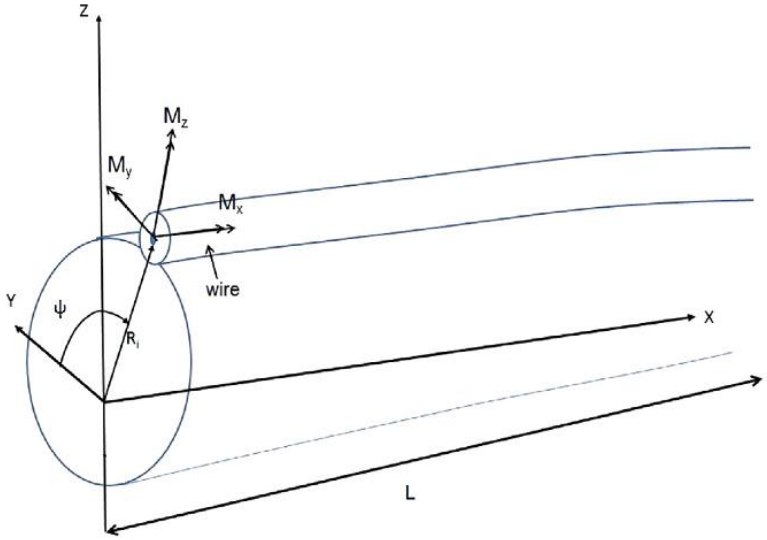

Figure 3.4: A simple conductor model [6]

Friction stress

The friction stress range can be calculated as the smallest stress range that is obtained from either the plane surfaces remain plain solution or the maximum allowed due to the friction between the interfaces, given by:

$$\Delta\sigma_f^i = \min\left(E\cos^2\alpha_i\, R_i\Delta\kappa, \frac{\pi R_i\tau_i}{\sin\alpha_i\, A_i}\right) \tag{3.14}$$

The expression for the maximum allowed due to friction is a result of integrating the available friction force per unit length τ_i along a quarter pitch length multiplied by 2 and divided by the area of the wire A_i. The friction force pert unit length is calculated by:

$$\tau_i \cong E\varepsilon_c\mu\left(\sum_{j=i+1}^{m}\frac{n_jA_j\cos^2\alpha_j\sin^2\alpha_j}{n_iR_j} + \sum_{j=i}^{m}\frac{n_jA_j\cos^2\alpha_j\sin^2\alpha_j}{n_iR_j}\right) \tag{3.15}$$

where μ is the coefficient of friction, ε_c is the strain resulting from the mean static tension *T,* given by:

$$\varepsilon_C = \frac{T}{EA_{\text{full}}} \tag{3.16}$$

4. Fretting

This chapter introduces the phenomenon of fretting. This is done in order to gain a better understanding of fretting, which may or may not contribute to a reduction of fatigue life of the conductor.

4.1 Introduction

According to [27] fretting is referred to as:

> *"A surface wear phenomenon occurring between two contacting surfaces having oscillating relative motion of small amplitude."*

Fretting fatigue is the combined effect of fretting and fatigue and often also include corrosion effects. The phenomenon can occur with less than 10 μm of relative motion between the mating surfaces. Major factors governing fretting fatigue are normal contact pressure between the mating surfaces, amplitude of the relative motion, frictional shear stresses between the mating surfaces, residual stresses, environment, material properties, load, frequency and the number of cycles [27].

4.2 Contact theory

The contact surfaces can behave in two ways:

1. The whole contact area slides (gross slip).
2. Some region of the contact area slides (partial slip).

In practise, most fretting problems do not involve gross sliding, here is the issue of wear often under control. It is therefore important to consider contacts where the shear force is less than the limiting frictional value [28].

If two bodies with curved surfaces are pressed together, they connect at a point or along a line. This results in an elastic or plastic flattening of the mating surfaces and this kind of contact is referred to as a Hertzian contact. The material close under the surface experiences tri-axial stress state and can due to this withstand higher stresses than yield stress [29].

The partial slip phenomenon is explained here with the example of two elastically similar cylinders. The cylinders are pressed together with a normal force *P,* which creates a Hertzian contact zone of semi width *a*. This zone has an elliptical distribution of normal pressure given by [28]:

$$p(x) = -p_0\sqrt{1-(x/a)^2} \tag{4.1}$$

If an increasing tangential force Q is applied so that it is less than the limiting factor of gross slip, $Q < \mu P$. The non-uniform pressure distribution causes a division of the contact zone into a slip and stick region as shown in Figure 4.1 [28].

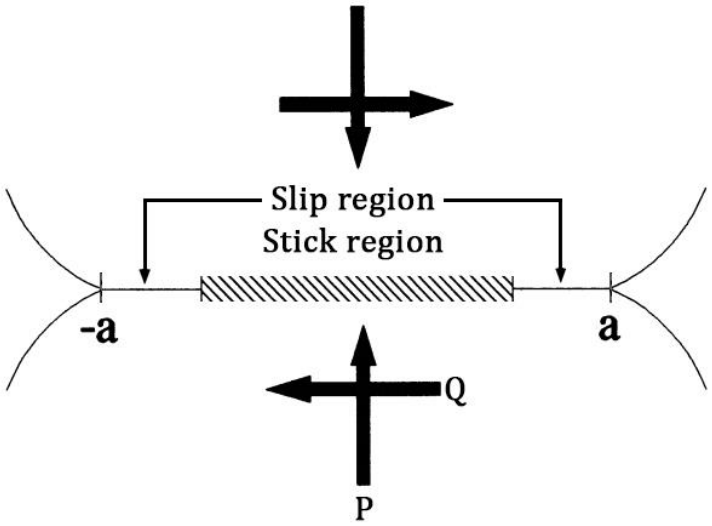

Figure 4.1: Slip and stick regions in a contact zone. Reproduced from [28]

Two slip zones will always be present at the ends, even if the shear force is small. The reason for this is as the normal pressure drops to zero, the required coefficient of friction must be infinite. A mathematical derivation proving this is given in [28] and by Johnson in [11], Johnson further noted that this is not surprising since the assumption of no slip requires two bodies to behave as one. For the case of two elastically dissimilar bodies, fretting can arise from a pure normal force only. This is due to different tangential displacement of the bodies which causes shear tractions [28].

Repeated sliding in the slip region leads to oxidation of the fretted surface, this causes wear debris formation and cracking. By investigation this region, a more worn out look compare to the rest of the contact area can be noticed [25]. Resistance to fretting fatigue generally decreases with higher hardness, and thereby with higher strength materials. Failures due to fretting fatigue results from micro cracks that arises in the fretting region and grows with cyclic stresses until fracture [27].

4.3 Fretting maps

It is practical to be able to determine the fretting regime based on experimental conditions. Vingsbo and Söderberg [30] suggested a fretting map model based on two variables with regime boundaries representing the critical transition values. Examples of fretting map variables are displacement amplitude, normal and tangential force and frequency of vibration. The model consists of four different regimes:

- *Stick regime*
- *Mixed stick-slip regime*

- *Gross slip regime*
- *Reciprocating sliding regime*

The *stick regime* has very limited surface damage by corrosion and wear. No fatigue crack growth is observed (up to 10^6 cycles) and low fretting damage is experienced. In the *mixed stick-slip regime*, wear and oxidation is noticeable but the effects are small. Accelerated crack growth may cause a strongly reduced fatigue life. Damage caused by this regime is referred to as fretting fatigue. The *gross slip regime* has severe surface damage, but crack formation is limited. This regime is often referred to as fretting wear and the surfaces can be in full sliding across each other. As the displacement amplitude increases, the gross slip approaches the *reciprocating sliding regime*. This leads to sliding wear.

The regime can be illustrated by a hysteresis loop in tangential force vs displacement diagram as shown in Figure 4.2. The stick regime is characterised in (a), it can be seen that for a low amplitude, the displacement is directly proportional to the tangential force. In the mixed stick-slip regime (b) a hysteresis loop is created where a small area between the lines represents the partial slip. For higher displacements, a larger area with a sudden drop of tangential force can be observed. This represents the gross slip regime (c).

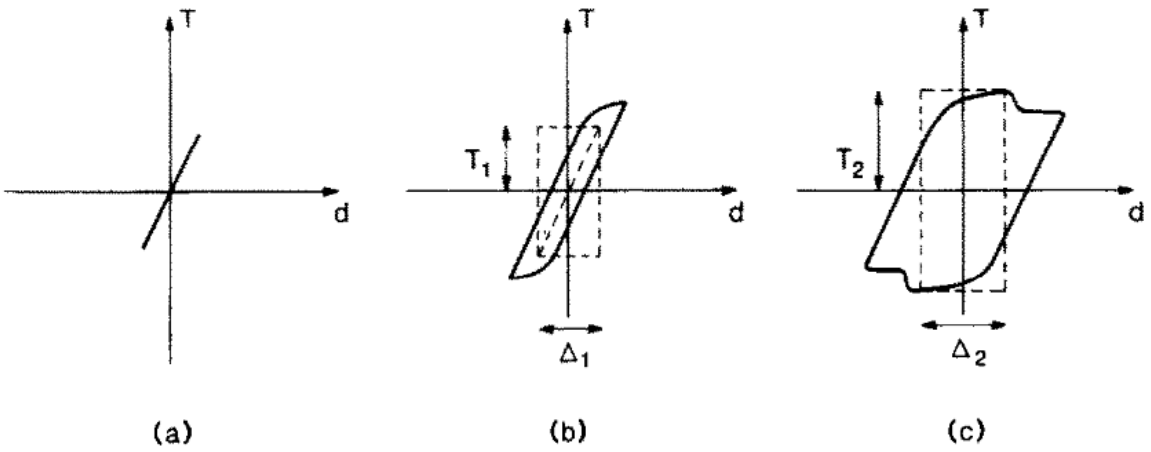

Figure 4.2: Tangential force vs displacement. (a) Stick regime, (b) Mixed stick-slip regime, (c) Gross slip regime

The study combined data from several other studies and a fretting map was suggested, see Figure 4.3. It can be seen that for low amplitudes in the mixed stick and slip regime, the wear rate is low. As the gross slip regime is entered, the wear rate increases until its levels of in the reciprocating sliding regime. The study also points out and shows in the figure that the fatigue life decreases with an increasing slip amplitude until a certain value. The reason for this is according to Novell and Hills [31] debatable, their study points out two possible reasons for this. 1. The increase in wear rate wears out embryo cracks before they can propagate. 2. A study [32] suggest that wear debris itself forms a solid lubricant layers, and thereby reduces stresses.

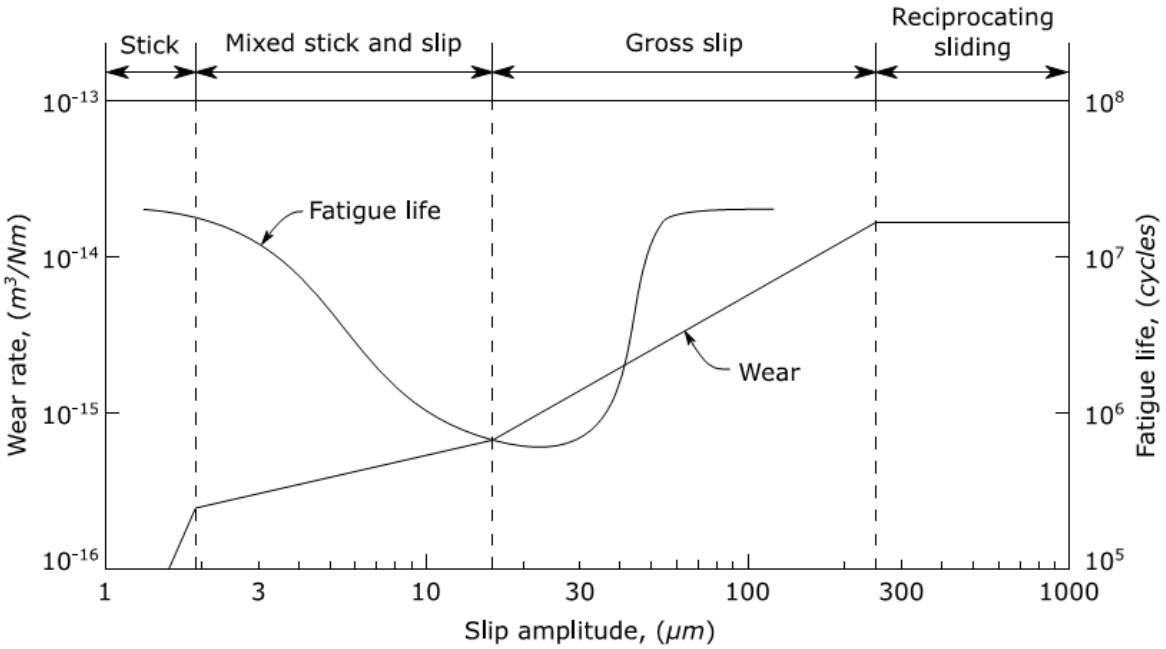

Figure 4.3: Fretting map [33]

5. Finite Element Analysis

This chapter introduces an overview of the finite element method, which is used in this work for solving structural problems. This is done by the use of BFLEX software which is described together with its methods.

5.1 Overview of the Finite Element method

The finite element method (FEM) is a numerical method to solve partial differential equations. The method is widely used in engineering for solving problems which are too complex to solve analytically. The basic concept is to discretize a system or a structure into a finite number of elements, where each element consists of a number of nodes. This is known as meshing. The unknow displacement field of a structure is thereby an approximation and described by the nodes. The displacements field between the nodes are interpolated, usually by linear, quadratic or cubic interpolation.

A stiffness relationship is established for each element using the principle of virtual displacement and the assumed displacement field. This yields an equilibrium between element forces, moments and displacements on the following form:

$$\boldsymbol{S} = \boldsymbol{kv} + \boldsymbol{S^0} \tag{5.1}$$

where $\boldsymbol{S}$ is the generalized nodal point forces, $\boldsymbol{k}$ is the element stiffness matrix, $\boldsymbol{v}$ is the nodal point displacements and $\boldsymbol{S^0}$ is the equivalent nodal point forces due to element loads.

A system stiffness relationship is then established by demanding equilibrium of all nodal points in the structure, the relationship is given by:

$$\boldsymbol{R} = \boldsymbol{Kr} + \boldsymbol{R^0} \tag{5.2}$$

where $\boldsymbol{R}$ is a vector containing all the nodal point forces of the structure. The system stiffness matrix $\boldsymbol{K}$ is established by the sum of the element stiffness matrices and $\boldsymbol{r}$ is the unknown global displacements vector. The system nodal force vector $\boldsymbol{R^0}$ is obtained from the equivalent element nodal point forces.

Once the system relationship is established, boundary conditions are introduced, which allows the global displacement vector to be solved for. The displacements are then used to calculate stresses in the structure by material laws.

Finite Element Analysis is solved by computers, accuracy depends on the number of elements which is a cost of computer time.

5.2 BFLEX

In this work, the BFLEX2010 FEA software has been used to model and solve for stresses in the conductor with finite element analysis. The software is based on the principle of virtual displacements, kinematic compatibility, material law and displacement interpolation. Also, nonlinear behaviour is considered. BFLEX was developed by the department of structural engineering at SINTEF Ocean with the purpose to:

- "provide a tool for stress and fatigue analysis of flexible pipes that both covers the cases where longitudinal stresses are insignificant and cases where such effect are important."

- "provide a tool for local buckling analysis of flexible pipes armour wires by building a model for all layers and allow for arbitrary motion of the wires."

The system architecture of BFLEX2010 is given by Figure 5.1 and the modules are:

- BFLEX2010. Analysis module.
- BFLEX2010POST. Postprocessing module.
- PLEX. Beam stress analysis of pressure spirals.
- BOUNDARY. Transverse stress analysis of pressure spirals.
- LIFETIME. Fatigue analysis.
- BPOST. The local model postprocessing module.
- XPOST. Graphical user interface for result visualization.

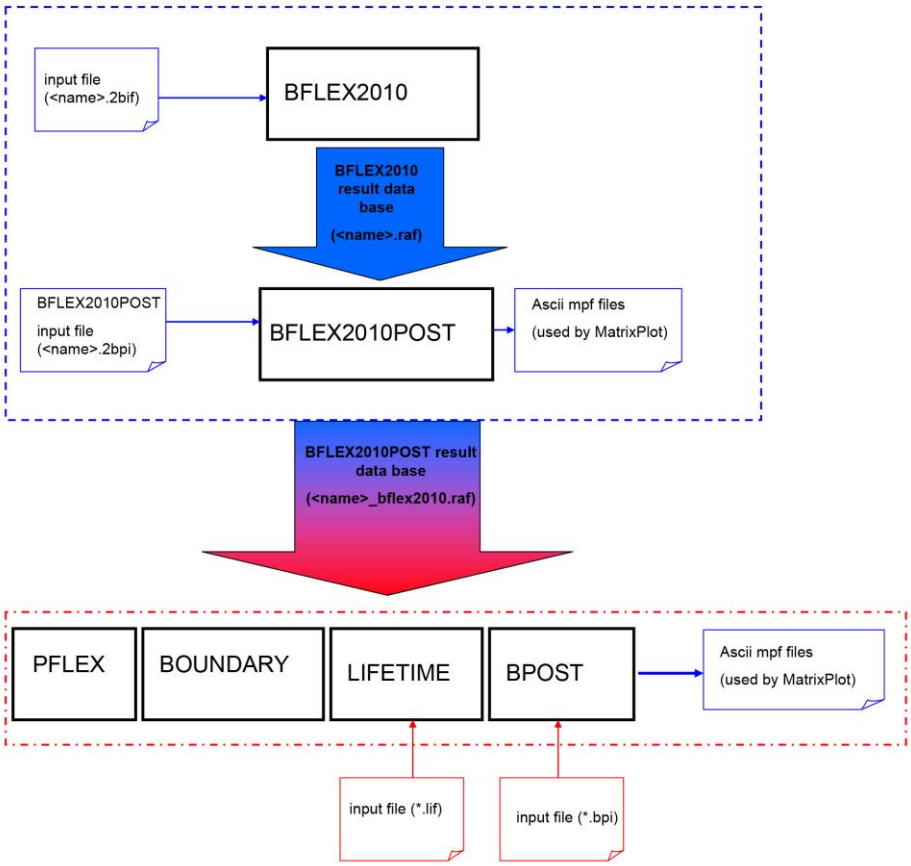

Figure 5.1: BFLEX system architecture

5.3 Principle of virtual displacement

The principle of virtual displacement or principle of virtual work basically states that the sum of internal work equals the sum of external work of the system. The general formula excludes volume forces and is given by [23]:

$$\int_V (\rho \ddot{\boldsymbol{u}} - \boldsymbol{f}) \cdot \delta u dV + \int_V \boldsymbol{\sigma} : \delta \boldsymbol{\varepsilon} dV - \int_S \boldsymbol{t} \cdot \delta \boldsymbol{u} dS = 0 \tag{5.3}$$

where ρ is the material density, $\ddot{\boldsymbol{u}}$ is the acceleration field, $\boldsymbol{f}$ is the volume force vector, $\boldsymbol{\sigma}$ is the Cauchy stress tensor, $\boldsymbol{\varepsilon}$ is the natural strain, $\boldsymbol{t}$ is the surface traction and $\boldsymbol{u}$ is the displacement vector. The first term in the equation is related to the inertial force, the second term is work done by internal forces and the last term corresponds to work done by external forces for the assumed displacement. BFLEX uses 2nd Piola Kirchhoff stress and the green strain tensor.

To solve problems with large deformation and with none-linarites, principle of virtual displacement has to be done on incremental form. Two common formulations are used, total Lagrange (TL) and updated Lagrange (UL), the difference between them is the choice of reference configuration. Total Lagrange refers to the initial configuration (C_o) and updated Lagrange refers to last obtained equilibrium configuration (C_n).

BFLEX uses a co-rotational formulation (CTL), this is a mixture of the total and the updated Lagrange formulation. This formulation separates rigid body motion from local or relative deformation of the element. To achieve this, a local coordinate system is attached to the element that continuously translates and rotates with the element during the deformation. This formulation is shown in Figure 5.2. The initial configuration C_o is the reference point, each element has C_{on} as its local coordinate system and C_n describes the deformation of the element.

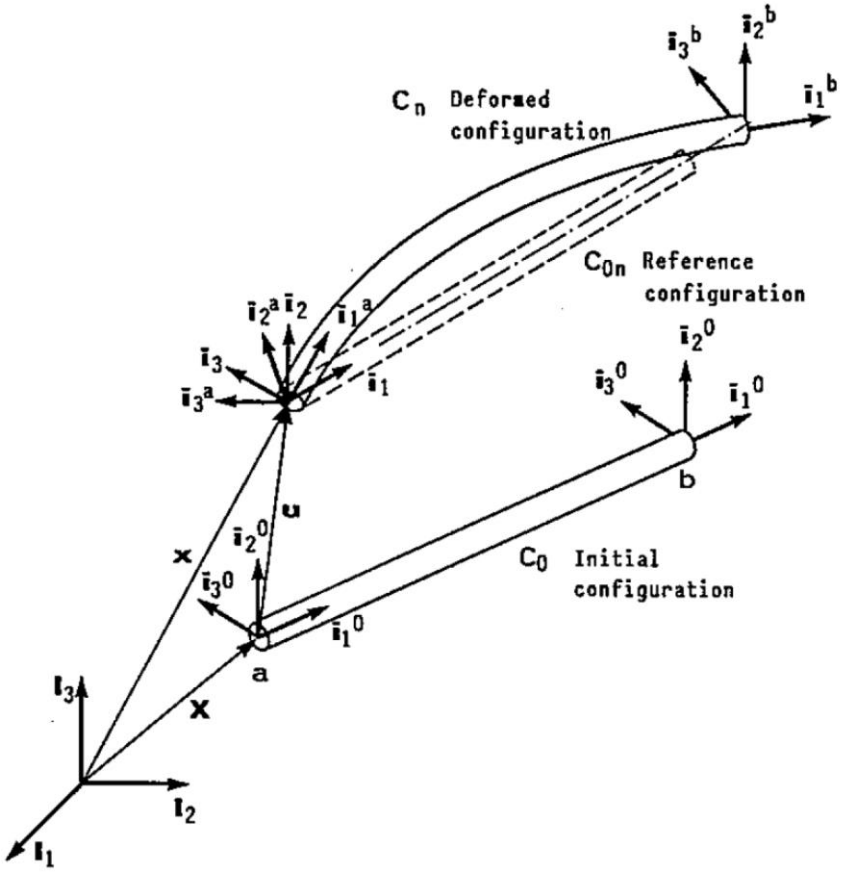

Figure 5.2: Co-rotational formulation [23]

The following three points are needed to implement the principle of virtual displacement into a numerical code.

1. Kinematic description. A relation between the displacement and rotations and the strains at a material point.

2. A material law connecting the strain with resulting stresses.

3. Displacement interpolation, describing the displacement and rotation fields by a number of unknowns on matrix format.

5.4 Nonlinear analysis

Nonlinear analysis is used when the displacement cannot be expressed as a linear function of the external load. This analysis has to be solved incrementally where the stiffness matrix is updated for each load step. There are generally three sources of nonlinearities [34, 35]:

- *Geometric nonlinearities.* This nonlinear effect is due to the change geometry as the structure deforms under a load. This is also referred to as large displacement analysis.

- *Material nonlinearities.* The relationship between strains and stresses is only linear until a certain limit, referred to as the yield strength of the material. Once stresses of this limit are exceeded, the material law changes from linear to non-linear. This is further explained in the next section.

- *Boundary conditions/contact.* Boundary nonlinearity occurs when displacement of the structure leads two surfaces into or out of contact. Stresses and displacements of bodies in contact are usually not linear dependent on the applied loads. This may occur even for small displacements and were the material behaviour is assumed to be linear, due to the fact that the contact area is usually not linear dependent on the applied loads. Friction effects causes a stick and slip behaviour of the contact areas and adds a further nonlinear complexity.

5.5 Material Model

As the stresses exceeds the elastic limit of the material an elastic-plastic formulation is required. There are three major features that governs the plasticity and are described here for a one-dimensional stress case [35]:

- *A yield condition or yield surface.* The condition defines which combinations of multi-axial stresses causing the material to be plastic.

- *A flow rule.* A relation between stress increment history to the plastic strain and the stress rate.

- *A hardening rule.* Describes how the yielding changes by historical plastic flow.

The *yield condition* states that yielding begins when the stress reaches its tensile yield strength. However, the level of stress needed to continue yielding, changes as the material yields and exceeds the initial level.

The *flow rule* can be written in multidimensional problems. For a one-dimensional stress case it leads to the relation $d\sigma = E_T(\varepsilon)d\varepsilon$.

The *hardening rule* describes how the yield condition changes by historic plastic flow. The two common methods used are kinematic and isotropic hardening. In kinematic

hardening the yielding occurs after unloading of $2\sigma_y$ whereas in isotropic hardening, the material remembers the hardening that already has occurred. For common metals, kinematic hardening model has better results. The two methods are shown in Figure 5.3.

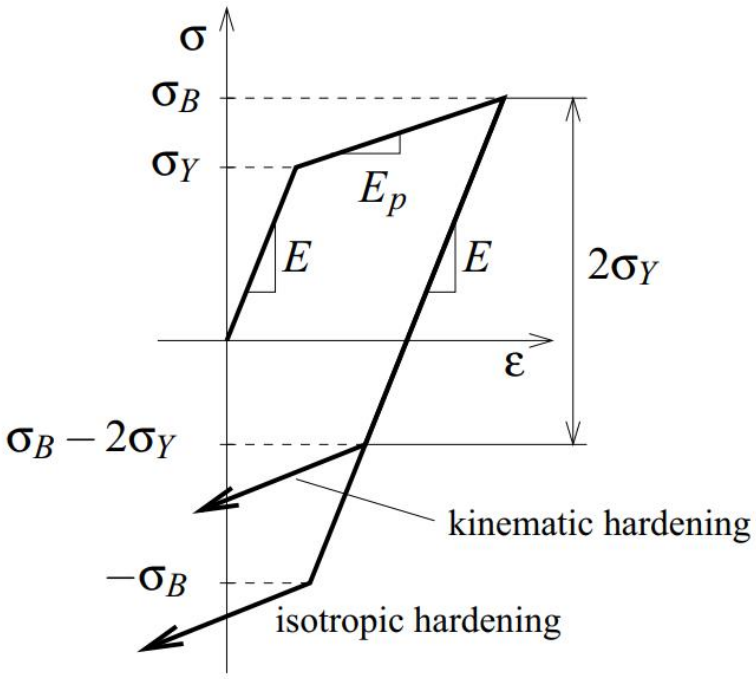

Figure 5.3: Hardening rules [36]

5.6 Solution procedure

BFLEX solves nonlinear problems by load incrementation with Newton-Raphson iteration. This is a common method is engineering and works well until one is dealing with extreme nonlinear problems where other methods such as the arc-length methods is needed.

5.6.1 Static analysis

The static solution procedure is based on Newton-Raphson iteration at each load step, the iteration procedure is according to:

$$\Delta \boldsymbol{r}_{\boldsymbol{k+1}}^{\boldsymbol{i}} = \boldsymbol{K}_{T,k+1}^{-1i} \Delta \boldsymbol{R}_{k+1}^{i} \tag{5.4}$$

where $\boldsymbol{K}$ is the global stiffness matrix, $\Delta \boldsymbol{R}$ is the load increments and $\Delta \boldsymbol{r}$ is the displacement increments. The load vector and the stiffness matrix are updated at each load step and the procedure is repeated until convergence is obtained. Newton-Raphson iteration for a system with 1 degree of freedom is shown in Figure 5.4 [23].

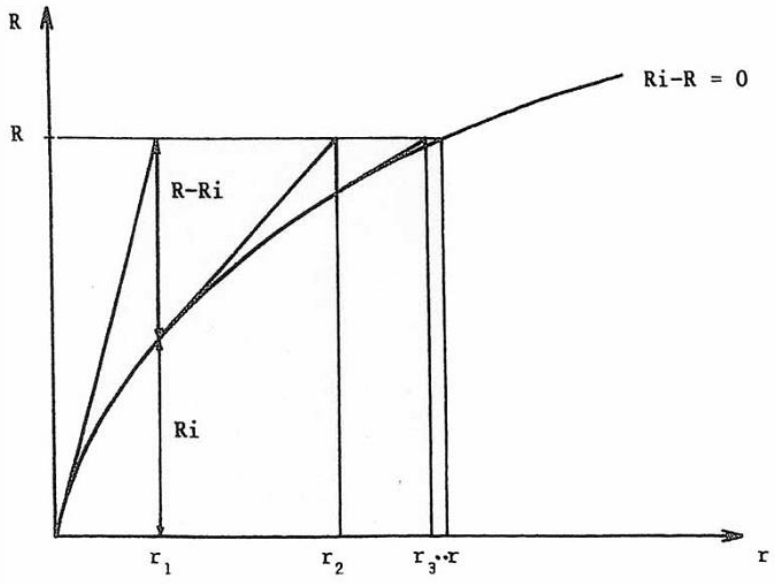

Figure 5.4: Newton-Raphson iteration [34]

5.6.2 Dynamic analysis

The dynamic solution procedure works in the same way as the static but is time dependent and considers inertia forces and damping in the structure. A step by step approach is used and the time interval is divided into smaller sub-intervals. At the beginning of a sub-interval are the displacement, velocity and acceleration known. By assuming the acceleration over the time step, the solution can be calculated for the end of the interval. The equilibrium equation of forced motion is defined as:

$$\boldsymbol{M}\ddot{\boldsymbol{r}} + \boldsymbol{C}\dot{\boldsymbol{r}} + \boldsymbol{K}\boldsymbol{r} = \boldsymbol{Q}(t) \tag{5.5}$$

where $\boldsymbol{M}$ is the global mass matrix, $\boldsymbol{C}$ is the global damping matrix, $\boldsymbol{K}$ is the global stiffness matrix and $\boldsymbol{Q}$ is the global load vector. To perform dynamic analysis, direct time integration is needed, this can be done by either explicit or implicit methods. Explicit methods are typically expressed as:

$$\boldsymbol{r}_{k+1} = \boldsymbol{f}(\ddot{\boldsymbol{r}}_k, \dot{\boldsymbol{r}}_k, \boldsymbol{r}_k, \boldsymbol{r}_{k-1}, \dots) \tag{5.6}$$

For explicit methods, the displacement at the next time step will be determined by the information of the current and previous time steps. The explicit method is conditionally stable and small time-steps are therefore required. This method is suitable for impulse analysis where small time steps are needed.

For implicit methods, the displacement at the next time step depends on quantities of the current and next time step, expressed as:

$$\boldsymbol{r}_{k+1} = \boldsymbol{f}(\ddot{\boldsymbol{r}}_{k+1}, \ddot{\boldsymbol{r}}_k, \dot{\boldsymbol{r}}_{k+1}, \dot{\boldsymbol{r}}_k, \boldsymbol{r}_k \dots) \tag{5.7}$$

Since information of the next time step is used, the acceleration of the system must be assumed between the time steps. Using information of the next step also results in a better numerical stability than for the explicit methods. The acceleration is assumed by different methods and some basic examples are the methods of constant acceleration, linear acceleration and constant initial acceleration. The Newmark β method is often used with different λ and β values to represent these different methods [37].

Newmark's $\boldsymbol{\beta}$

The following equations describes the Newmark β-family, including the Wilson θ −method considering a constant time step in the analysis. The methods relate the displacement, velocity and acceleration vectors at time t and t + $\Delta\tau$.

$$\dot{\boldsymbol{r}}_{\boldsymbol{t}+\Delta\boldsymbol{\tau}} = \boldsymbol{r}_{\boldsymbol{t}} + (1-\gamma)\ddot{\boldsymbol{r}}_{\boldsymbol{t}}\Delta\boldsymbol{\tau} + \ddot{\boldsymbol{r}}_{\boldsymbol{t}+\Delta\boldsymbol{\tau}} \tag{5.8}$$

$$\boldsymbol{r}_{t+\Delta\boldsymbol{\tau}} = \boldsymbol{r}_t + \dot{\boldsymbol{r}}_t\Delta\boldsymbol{\tau} + \left(\frac{1}{2}-\beta\right)\ddot{\boldsymbol{r}}_{\boldsymbol{t}}(\Delta\boldsymbol{\tau})^{\boldsymbol{2}} + \beta\ddot{\boldsymbol{r}}_{\boldsymbol{t}+\Delta\boldsymbol{\tau}}(\Delta\boldsymbol{\tau})^{\boldsymbol{2}} \tag{5.9}$$

Where $\Delta\tau = \theta\Delta t,\ \theta \geq 1$.

The parameters γ , β and θ defines the functional change in displacement, velocity and acceleration vectors over the time step Δt. For the Newmark β-family, $\theta = 1$, this gives by change of parameters γ and β the different methods within the Newmark β-family [38, 39].

Dynamic analysis results in a series of modes with different frequencies. Usually are only the modes with low frequency of interest and it is therefore desirable to remove the other modes. The medium modes are eliminated by increasing the damping ratio or introducing Rayleigh-damping to the Newmark β method, leaving the lower and the higher modes unaffected. The higher modes can be damped out by numerical damping, this will reduce the accuracy in the Newmark β method.

Modified Hilbert-Hughes-Taylor method

The modified Hilbert-Hughes-Taylor method (HHT-α method) is used in BFLEX and does not suffer from reduced accuracy when the high modes are damped out. The modified equilibrium equation is given by [39]:

$$\begin{aligned}\boldsymbol{M}\ddot{\boldsymbol{r}}_{k+1} + (1+\alpha_H)\boldsymbol{C}\dot{\boldsymbol{r}}_{k+1} - \alpha_H\boldsymbol{C}\dot{\boldsymbol{r}}_k + (1+\alpha_H)\boldsymbol{R}^{\boldsymbol{I}}_{k+1} - \alpha_H\boldsymbol{R}^{\boldsymbol{I}}_k \\ = (1+\alpha_H)R^{\boldsymbol{E}}_{k+1} - \alpha_H\boldsymbol{R}^{\boldsymbol{E}}_k\end{aligned} \tag{5.10}$$

where $\boldsymbol{M}$ is the mass matrix, $\boldsymbol{C}$ is the damping matrix $\boldsymbol{R^I}$ is the internal force vector, $\boldsymbol{R^E}$ is the external force vector and α is a constant. The damping matrix $\boldsymbol{C}$ includes both Rayleigh and diagonal damping. The method is unconditionally stable when [23]:

- $-\frac{1}{3} \leq \alpha_H \leq 0$
- $\gamma = \frac{1}{2}(1 - 2\alpha_H)$
- $\beta = \frac{1}{4}(1 - \alpha_H)^2$

5.6.3 Convergence criteria

The iteration algorithm stops when equilibrium of a certain tolerance level is reached, this is achieved by a vector norm, which is a measure of the size of the vector. Norms based on displacement, energy and forces can be used.

BFLEX runs on a predefined number of iterations and divisions. If no convergence is reached for the first iterations cycle, it divides the time-step and starts a new trial. This process repeats until convergence is reached or stops after the specified number of divisions is reached.

5.7 Elements formulation

In the model are different types of elements used depending on what degrees of freedom that is needed. The elements used in this model are presented in the following and the theory is taken from the BFLEX theory manual [23].

5.7.1 PIPE31

The PIPE31 element is a standard 3D beam element. It has two nodes and 6 degrees of freedom in each node, 3 translational and 3 rotational. The stresses under plane stress are according to Hooke's law:

$$\begin{bmatrix} \sigma_{11} \\ \sigma_{22} \\ \tau \end{bmatrix} = \left(\frac{E}{1-\nu^2}\right) \begin{bmatrix} 1 & \nu & 0 \\ \nu & 1 & 0 \\ 0 & 0 & \dfrac{1-\nu^2}{2(1+\nu)} \end{bmatrix} \begin{bmatrix} \varepsilon_{11} \\ \varepsilon_{22} \\ \gamma \end{bmatrix} \tag{5.11}$$

The displacement of an arbitrary point is given by:

$$u_1(x, y, z) = u_{1,0} - yu_{2,0} - zu_{3,0} \tag{5.12}$$

$$u_2(x, y, z) = u_{2,0} - z\theta_x \tag{5.13}$$

$$u_3(x, y, z) = u_{3,0} - y\theta_x \tag{5.14}$$

Where $\sigma_{i,j}$ is the stress in the *i, j* direction, ν is the Poisson's ratio, $\varepsilon_{i,j}$ is the strain in the *i, j* direction, γ is the shear strain, u_i is the displacement in i direction and θ is the rotation.

5.7.2 HSHEAR363

The HSHEAR363 element is similar to a standard beam element (PIPE31). Compare to a standard beam element, one additional node is included to describe radial motion of the layer. The additional node includes 3 degrees of freedom, but since only the radial DOF is used the other two has to be supressed. The purpose of the element is to handle plastic layers, pressure armour layers and tape layers.

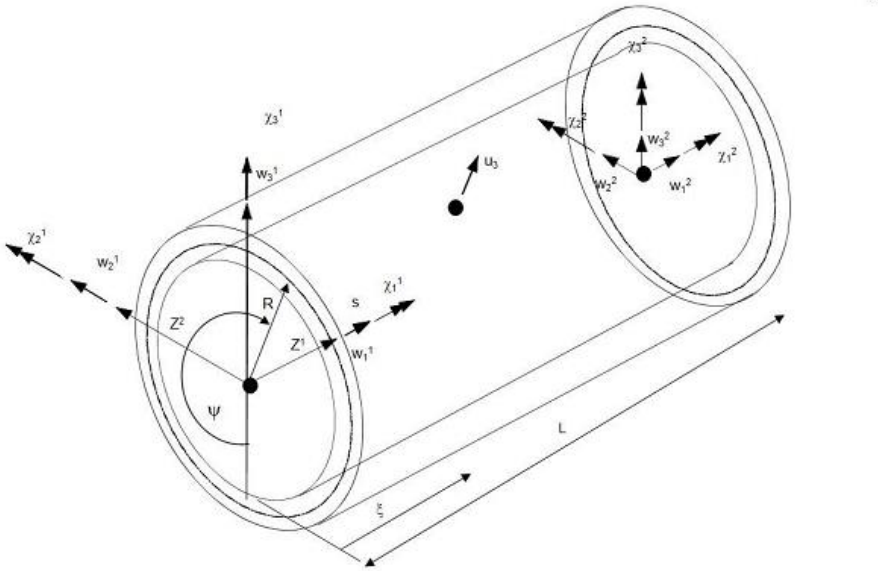

Figure 5.5: HSHEAR363 Element

5.7.3 HSHEAR353

The HSHEAR353 element is a curved beam element with 26 degrees of freedom and 4 nodes that it is used to model helices. In addition to the 12 standard DOFs at the centreline used to model global strain quantities, 12 are used to describe the local displacement of the wire relative to the core and 2 are used to describe the longitudinal slip process. However, the torsion DOF at the helix nodes has to be suppressed due to kinematic constraints and thereby are only 24 DOFs active.

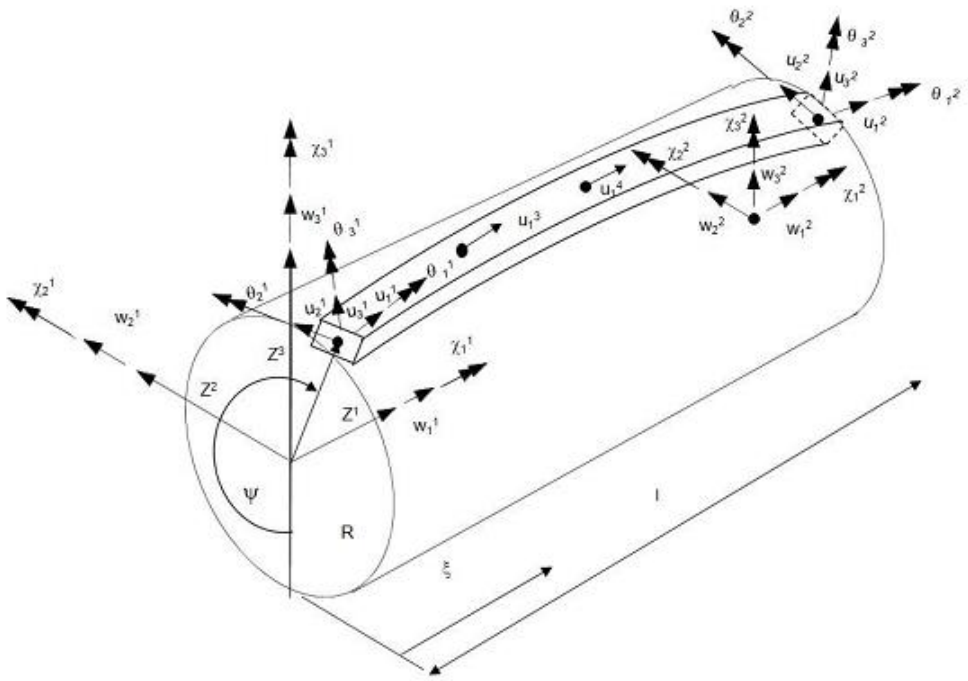

Figure 5.6: HSHEAR353 Element

The kinematics of the element is described in the following with respect to Figure 5.7. The strains can be described by:

$$\varepsilon_1 = u_{1,1} - \kappa_3 u_2 + \kappa_2 u_3 \tag{5.15}$$

$$\varepsilon_2 = u_{2,1} - \kappa_3 u_1 + \kappa_1 u_3 \tag{5.16}$$

$$\varepsilon_3 = u_{3,1} - \kappa_2 u_1 + \kappa_1 u_2 \tag{5.17}$$

Rotations can be described by:

$$\omega_1 = \kappa_1 u_{1,1} - \kappa_t u_{2,1} + \kappa_3\left(u_{3,1} + \kappa_1 u_2\right) + \kappa_2\left(u_{2,1} - \kappa_1 u_3\right) + \omega_{1p} \tag{5.18}$$

$$\omega_2 = u_{3,11} - \kappa_2 u_{1,1} - 2\kappa_1 u_{2,1} - \kappa_3 \kappa_t u_2 + \kappa_1 \kappa_1 u_3 + \omega_{2p} \tag{5.19}$$

$$\omega_3 = u_{2,11} - \kappa_3 u_{1,1} - 2\kappa_1 u_{3,1} + \kappa_2 \kappa_t u_2 - \kappa_1 \kappa_1 u_2 + \omega_{3p} \tag{5.20}$$

where:

$u_{i,j}$: the differentiation of the displacement components u_i along X^i with respect to the curvilinear coordinate X^J.
ε_1: First order axial strain
ε_2: Centreline rotations about X^3 axis
ε_3: Centreline rotations about X^2 axis
ω_1: Centreline torsion
ω_2: Curvature about X^2 axis

ω_3: Curvature about X^3 axis
ω_{ip}: The quantities represent the prescribed torsion and curvature quantities from bending.
κ_1: Initial total accumulated torsion of the cross-section centreline
κ_2: Initial accumulated curvature in the X^1- X^3 plane
κ_3: Initial accumulated curvature in the X^1- X^2 plane

In the initial state of the helix, from which ω_i and ε_i are measured:

$$\omega_i\ ,\ \varepsilon_i\ ,\kappa_1 = \frac{\sin\alpha\cos\alpha}{R},\ \ \kappa_2 = \frac{\sin^2\alpha}{R},\ \ \kappa_3 = 0 \tag{5.21}$$

The kinematic constraint describing the torsion rotation is given by:

$$\theta_1 = \kappa_1 u_1 - \kappa_t u_2 \tag{5.22}$$

which assumes that the wire follows the supporting surface with varying transverse curvature given by:

$$\kappa_t = \frac{\cos^2\alpha}{R} + \sin^2\alpha\left(\frac{-\omega_{2,11}\sin\psi}{1 - R\omega_{2,11}\sin\psi} + \frac{\omega_{3,11}\cos\psi}{1 + R\omega_{3,11}\cos\psi}\right) \tag{5.23}$$

where ω_i is the global displacement along the global axis Z^i.

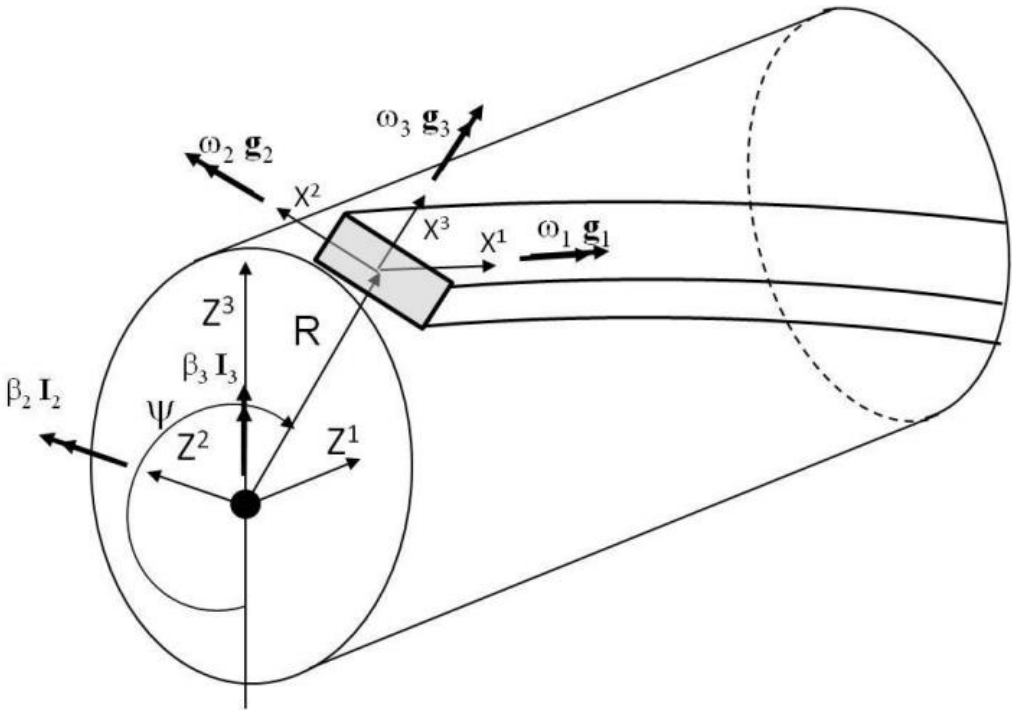

Figure 5.7: Kinematics of helix element

5.7.4 HCONT463

The HCONT463 element is a contact element with 13 degrees of freedom and 3 nodes, it is used to model contact between a cylindrical layer and a helix layer, i.e. between a HSHEAR363 and a HSHEAR353. Figure 5.8 illustrates how the HCONT463 element connects a HSHEAR363 (body A) element with a HSHEAR353 (body B) element. The HSHEAR353 element includes 3 translation directions and the HSHEAR363 includes only the radial displacement.

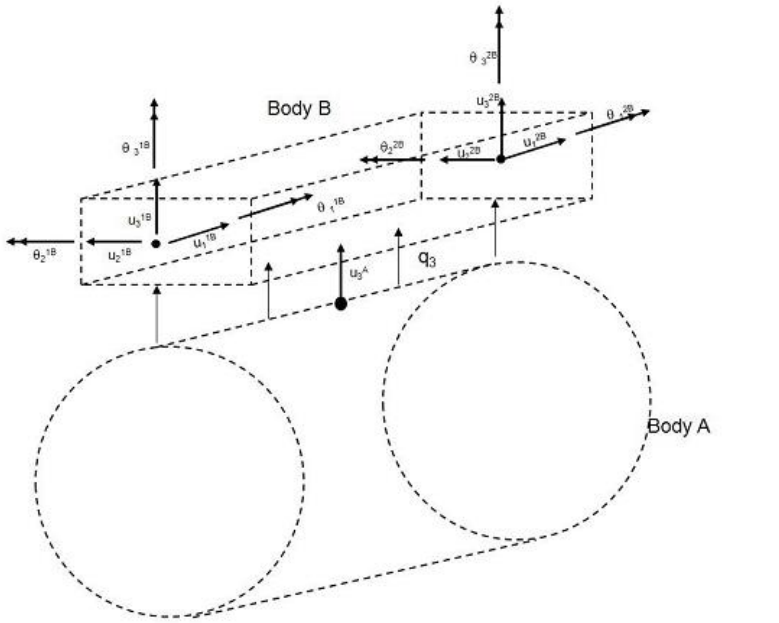

Figure 5.8: HCONT463 Element

5.7.5 HCONT454

The HCONT454 element is a contact element with 36 degrees of freedom and 6 nodes. It is used to model contact in the hoop direction within helical layers i.e. between HSHEAR353 elements.

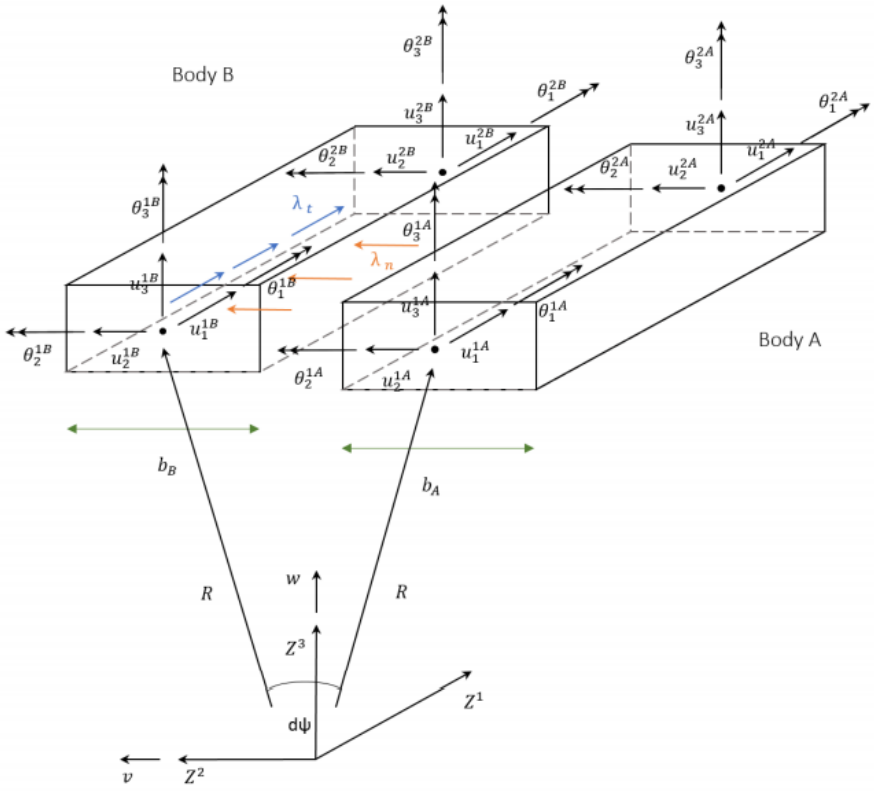

Figure 5.9: HCONT454 Element

6. Modelling and Simulation

In this chapter are the main parts of the modelling procedure and the simulation described.

6.1 Procedure

The conductor was modelled in with a full length of 3.24 meter, but due to computer limitations, it was truncated into a detailed part of the midsection. The detailed part was meshed with 100 elements per wire in the longitudinal direction. The two remaining parts, the ends, was modelled with 30 standard beam elements for each end.

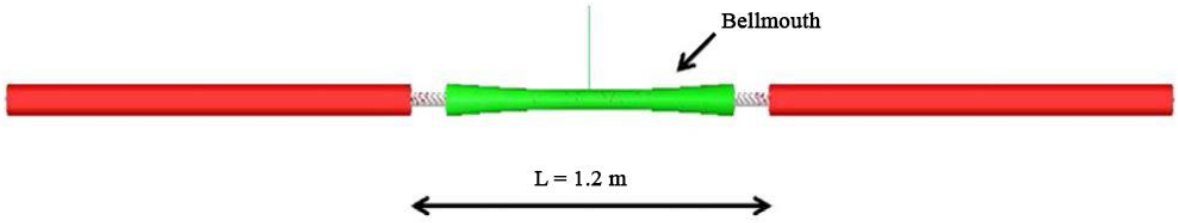

Figure 6.1: Illustration of the model

A tensile load of 30 kN was applied gradually by initial strain during the first second and then held constant. The conductor was then bent back and forward by the movement of a bellmouth with a prescribed displacement in order to simulate tension-bending loading. Figure 6.1 shows an illustration of the conductor inside the bellmouth. This was done for two radii of curvature, 3 and 6.5 meters. This results in an axial force history at the end beams as shown in Figure 6.2. The maximum dynamic forces are 32.2 kN and 30.4 kN for the 3 and 6.5-meter bellmouth, respectively. The stress ranges due to dynamic tension are based on these forces.

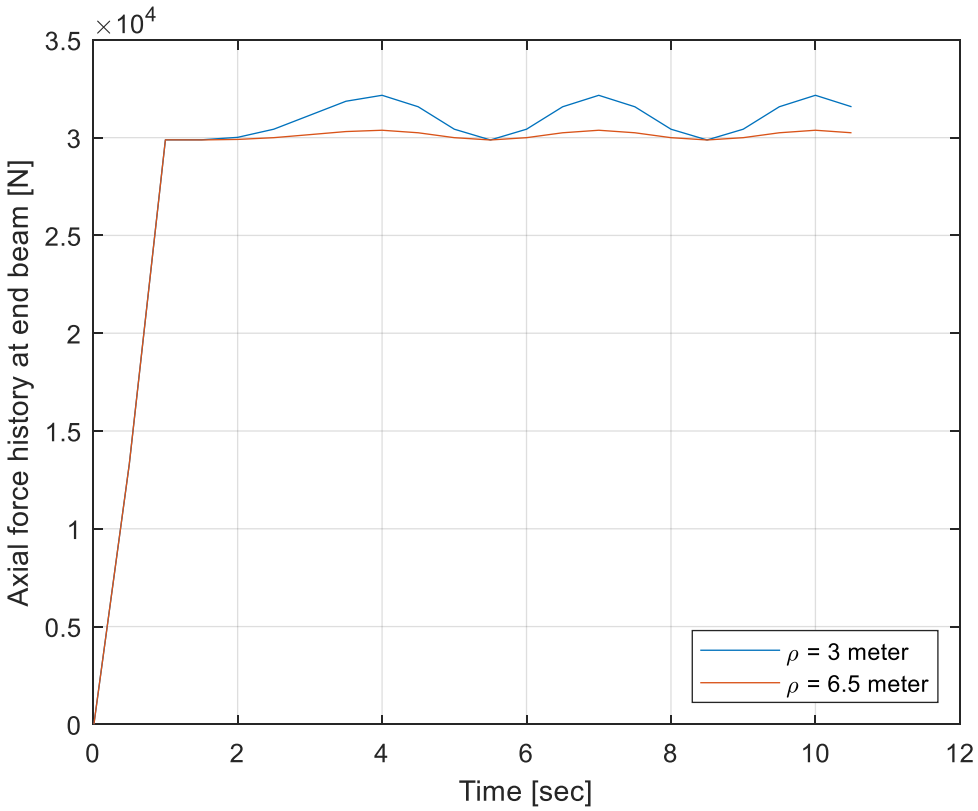

Figure 6.2: Axial force histories at end beams due to reversed bending.

Dynamic analysis was used with a time step of 0.001 seconds. Displacement, energy, and force norms of $1 \cdot 10^{-5}$ was used when possible and only the displacement norm when convergence was hard to reach.

The model is based on beam and beam contact elements with the idea that fatigue strength is mainly governed by longitudinal stresses. The local longitudinal stress is given by:

$$\sigma_{XX} = \sigma_{XX-AX} + \sigma_{XX-MY} + \sigma_{XX-MZ} \tag{6.1}$$

where σ_{XX-AX} is axial stress, σ_{XX-MY} is stress due to bending about the y-axis (weak axis) and σ_{XX-MZ} is stress due to bending about the z-axis (strong axis). SCFs due to the geometrical irregularities are applied in the fatigue set up.

The model and the simulation consist of three input files or codes, one for the model, one for the fatigue set up and one for post processing. The input file of the 3-meter radii model is given in appendix B, this is identical with the 6.5-meter model except for the radii of the bellmouth and the movement of it.

6.2 Cross-section definition

The conductor consists of 4 layers. Layer 1 is the core and consist of 1 wire, layer 2, 3 and 4 are helical layers and consist of 6, 12 and 18 wires, respectively. In order to model the conductor with the chosen elements, artificial tape layers have to be introduced between layer 2 and 3, 3 and 4, and outside layer 3. This means that the trellis contact is not modelled as a point contact, instead, it is a smooth distributed contact. The helical layers have a lay angle of 4.33°, -8.03° and 11.56° for the 2nd, 3rd and 4th layer, respectively.

The core and the tape layers are modelled with HSHEAR363 and the helical layers with HSHEAR353 elements. Inline contact is modelled with HSHEAR454. Contact between the core and layer 2 and contact between helical layers and tape layers are modelled with HCONT463.

6.3 Material data

The copper material is defined in BFLEX for the cross-section of a wire. There are 37 wires and each wire have a cross section of 8.11 mm^2. The material data is presented in Table 3 and Table 4.

Table 3: Material data of structural elements

Property	Copper	Plastic
Type	Linear	Elastic
Young's modulus [GPa]	115	0.7
Shear modulus [GPa]	0.42	-
Poison's number [-]	0.355	0.35
Axial stiffness [N]	932650	-
Bending stiffness [Nm^2]	0.6	-
Bending stiffness [Nm^2]	0.6	-
Torsional stiffness [Nm^2]	0.44	-

The shear stiffness of the axial contact elements has to be set with sufficient stiffness to reflect the plane surfaces remain plane condition. The minimum value recommended for a helix element is given by [40]:

$$10\frac{EA}{R_i^2}sin^2\,\alpha_i \tag{6.2}$$

where R_i and α_i is the radius and the lay angle of the layer, respectively. The results of this is shown for each layer in Table 4.

Table 4: Material data of contact elements

Property	Contact01
Type	Coulomb friction
Static friction coefficient [-]	0.2
Dynamic friction coefficient [-]	0.2
Elastic stiffness in axial direction [MN/m^2]	
-Layer 2	5159
-Layer 3	1298
-Layer 4	577

6.4 Boundary conditions

The degrees of freedom of the conductor's ends are fixed in all translation directions and in rotation about the x-axis. All the nodes of the helical layers are fixed in rotations about the x and y axis, and the end nodes are fixed in x and y translation as well. The nodes of the core and the tape layers are fixed in y and z translation.

It should be noted that the degrees of freedom do not reflect the displacement of the nodes. The elements are free to deform. The restriction is not in space, but relative to the supporting surface, this means that surfaces/elements instead sticks to each other.

6.5 Mesh Sensitivity & Length optimization

The initial length of the truncated conductor was 1.5 meter. By investigating the of curvature along the length of the conductor, it was found that this length was longer than needed. A length corresponding to a curvature of zero close to the ends is a better choice taking computational cost into account, this length was found to be 1.2 meter. Figure 6.3 shows the bending curvature along the length of the conductor at maximum deformed formation.

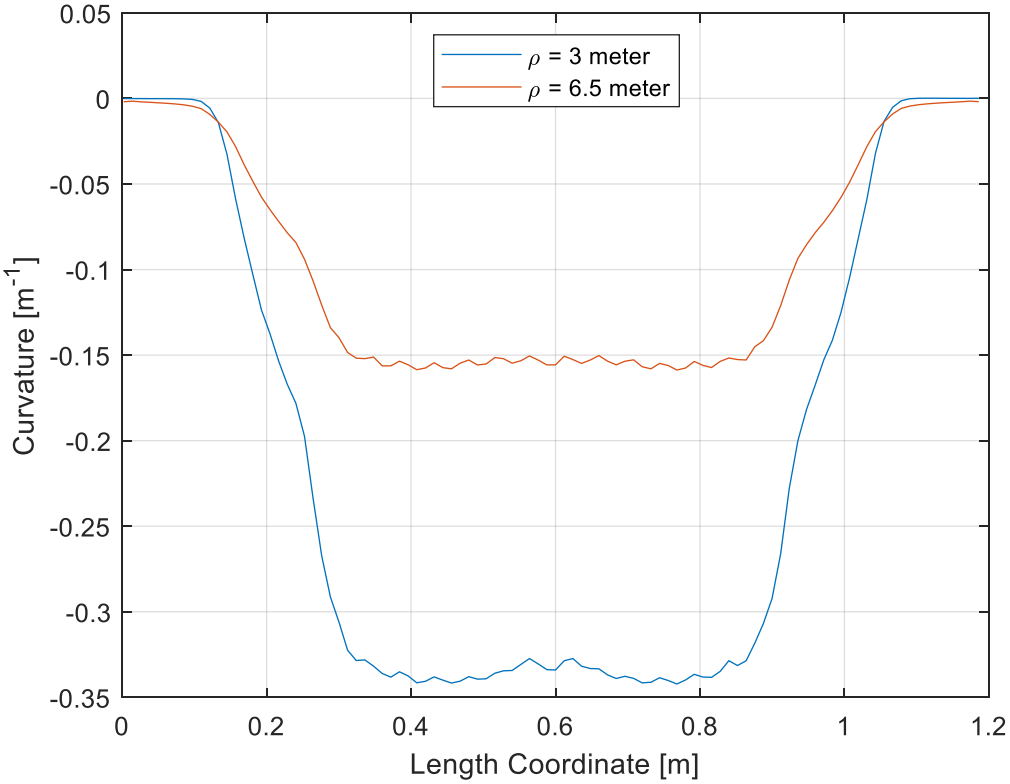

Figure 6.3: Bending curvature along the model at maximum deformation

Shortening of the conductor and keeping 100 elements per wire in the length direction servers as a mesh sensitivity study, doing so resulted in no significant different. To further validate this, the initial 1.5 m conductor was simulated with 150 elements to make sure no effects of changing the length was involved.

6.6 Fatigue set up

The SN-curve for single wires produced by Nasution et. al [7] was imported into to BFLEX. This curve is given by equation 3.7 and with the parameters of m = 8.424 and c = $2.88 \cdot 10^{25}$.

The stress concentration factors for each layer was specified, SCF = 1.08 for layer 4 and SCF = 1 for the other layers. When mean stress correction is considered it is handled by BFLEX with the given ultimate stress for copper as 315 MPa, taken from [6].

The fatigue life prediction is based on the maximum stress range found from when the conductor has reached maximum deformation and then one full bending cycle from there.

7. Results

This chapter presents the results.

7.1 Analytical model

The stress ranges were predicted with the analytical model presented in section 3.5 and given in Table 5.

Table 5: Summary of stress contribution predicted by the analytical model

Contribution	Analytical	Layer 3	Layer 4
Radius of curvature $\rho = 3$ m			
Dynamic tension	7	7	7
Friction	105	45	6
Bending stress in the y-direction	121	116	108
Total	232	167	121
Radius of curvature $\rho = 6.5$ m			
Dynamic tension	1	1	1
Friction	105	45	6
Bending stress in the y-direction	56	53	50
Total	162	99	57

7.2 Friction coefficient

The influence of the friction coefficient was investigated by performing several simulations. The results are shown in Table 6. It should be noted that this sensitivity study was performed with and axial stiffness of 400 MN/m^2 which is not used in the final results. The dry and lubricated friction coefficient corresponds to $\mu = 0.2$ and $\mu = 0.02$ respectively. It is clear that the friction coefficient has a strong influence on the stress and thereby the predicted life. All failures were found in the second layer except for the two cases with the lowest friction coefficient where they occurred in the fourth layer and the third layer with Goodman correction.

Table 6: Sensitivity study of friction coefficient

μ	$\Delta\sigma_{xx}$ [MPa]	No mean stress correction	Gerber	Goodman
		Bellmouth with radii of 3 meter:		
0.01	159 (L4)	8 276 227	8 562 303	7 337 134
0.02	158 (L4)	8 705 948	8 717 180	7 081 601
0.10	185	2 267 713	2 424 560	2 484 793
0.20	226	432 333	704 449	891 409
0.30	265	109 751	297 629	423 610
0.40	289	52 804	180 877	275 584
0.50	296	43 420	160 462	254 125
		Bellmouth with radii of 6.5 meter:		
0.2	134	35 058 196	25 732 408	19 544 305
0.5	171	4 371 203	3 967 482	3 760 049

7.3 Shear stiffness of contact elements

The shear stiffness of the contact element must be set with sufficient stiffness to reflect the plane surface remain plane condition. The simulation was first done with shear stiffness of 400 and 600 MN/m^2. These values are far less than the minimum recommended given by equation 7.2. At first, values from this formula resulted in no convergence, this was solved by only using the displacement norm. The result shows that the change of shear stiffness have some minor influence on the 3-meter radii model and a significant influence on the 6.5-meter radii model. The reason for this is that the 6.5-meter radii model is more in the stick domain which is governed by the parameter.

Table 7: Shear stiffness sensitivity

Shear stiffness MN/m^2	$\Delta\sigma_{xx}$ [MPa]	No mean stress correction	Gerber	Goodman
		Bellmouth with radii of 3 meter:		
400	226	432 333	704 449	891 409
600	229	385 405	652 468	838 490
Eq. 7.2	231	354 481	619 306	806 517
		Bellmouth with radii of 6.5 meter:		
400	134	35 058 196	25 732 408	19 544 305
600	141	22 239 865	17 393 694	14 227 543
Eq. 7.2	159	8 424 528	7 747 793	7 278 603

7.4 Friction forces

The friction force starts to develop as the conductor is being bent, it comes from contact between the different layers and hoop contacts within the layer. By plotting the forces (Figure 7.1) of a contact element vs time it can be seen that the contribution from hoop contact is small. This was done for different elements and it should be noted that for one element, "spikes" was found at certain time steps resulting in big jumps of the otherwise smooth curve. This is assumed to be due to some numerical error meaning the model is not totally stable.

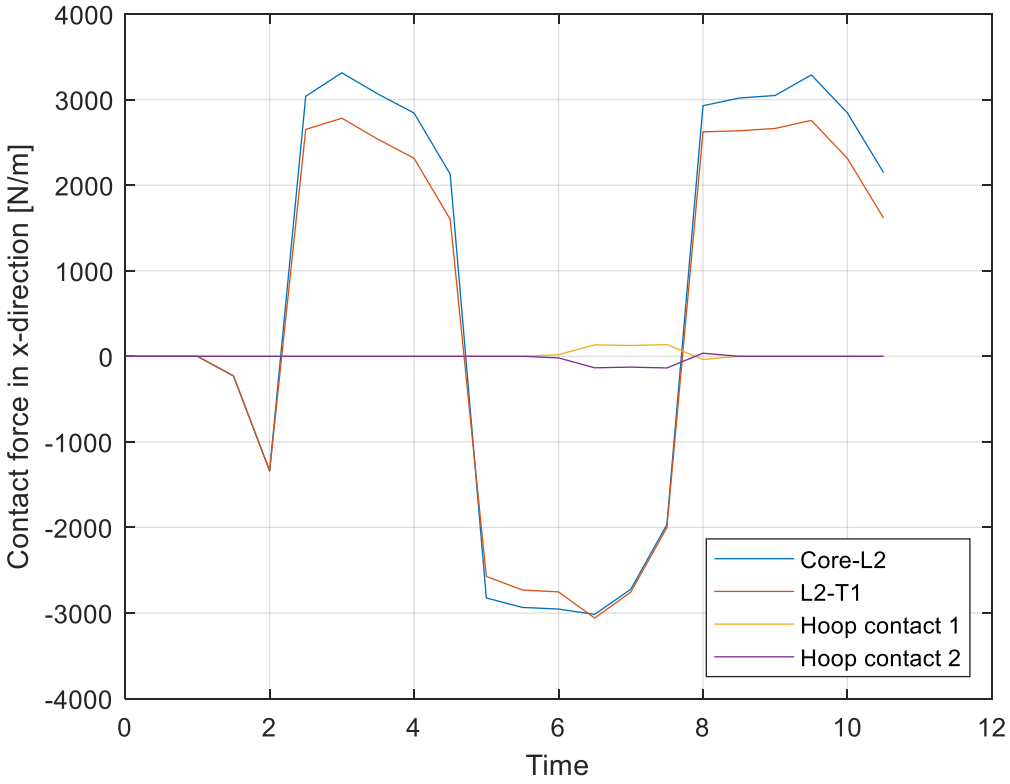

Figure 7.1: Contact forces vs time of an element

Removing the contact elements results in a higher stress range and thus a better prediction, as shown in Table 8. However, this result is not considered valid.

Table 8: Results with no hoop contact elements

$\Delta\sigma_{xx}$	No mean stress correction	Gerber	Goodman
245	211 933	435 974	576 897

7.5 Ultimate strength and mean stress correction

The ultimate strength of copper varies, values of 315 MPa and 250 MPa was investigated. The fatigue life of using the higher ultimate strength gives a shorter life for

the model with 3-meter radii bellmouth and longer life for the 6.5-meter model, using Goodman mean stress correction. This is because the correction depends on if the results of the stresses lies above or beneath the R-ratio of the SN-curve. As can be seen in Figure 7.2, the influence of ultimate stress and mean stress correction is small but significant for the model with 3 meter radii and almost non existing for the model with 6.5 meter radii. How the ultimate strength affects fatigue life with other or no mean stress correction is unknown.

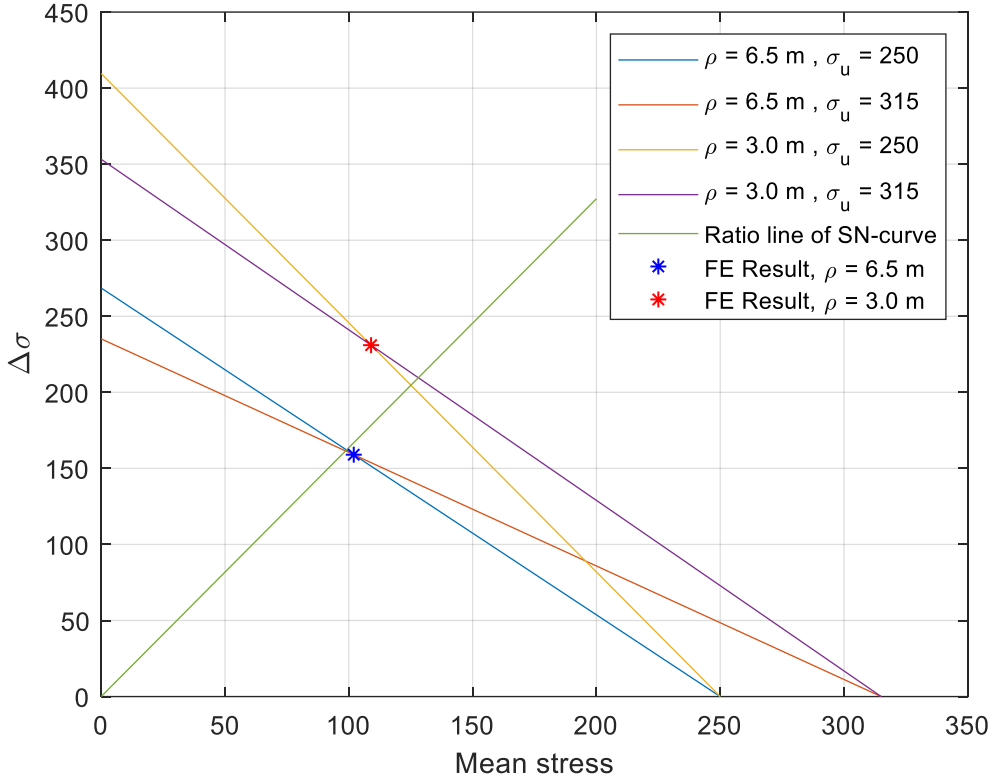

Figure 7.2: Influence of ultimate stress and Goodman mean stress correction

7.6 Predicted results vs laboratory tests

Considering the friction coefficient of $\mu = 0.2$, all predicted failures took place in the second layer inside the bellmouth (some distance off-centre) and was in good agreement with the analytical model. The predicted stress range was 231 and 159 MPa for the 3-meter radii and 6.5-meter radii, respectively and without mean stress correction. Figure 7.3 shows the predicted stress ranges compared with the results of the laboratory tests, it is clear that the model overestimates the fatigue life or underestimates the stress range. The latter implies that fatigue life is mainly governed by longitudinal stress range which is not necessarily true. In fact, the result suggests that the fatigue damage is induced by fretting.

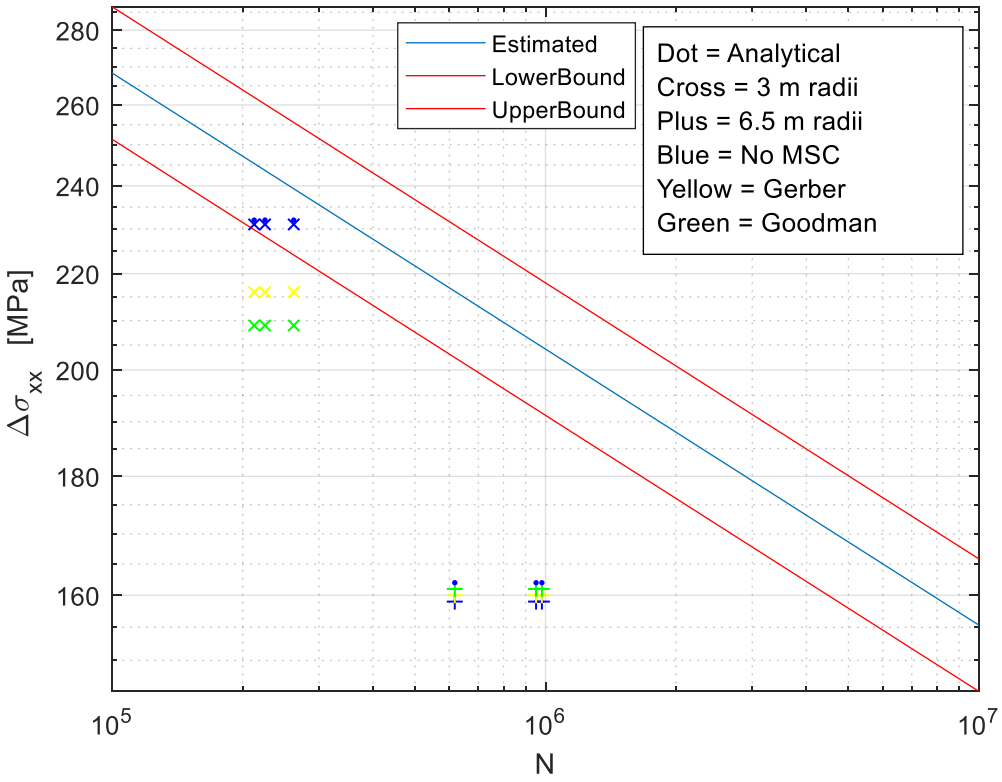

Figure 7.3: Cycles until failure of the laboratory tests vs predicted stress ranges

7.7 Indications of Fretting

The displacement amplitude is one major parameter governing fretting. In BFLEX this parameter corresponds to the relative displacement between wires. The displacement differs between layers, cross-section position and length coordinate. As a reference for the results presented in this section, the displacement amplitude is taken at the midsection of the conductor, and at the highest amplitude for each of the mating surfaces. Table 9 shows the results of the two models. Comparing these results with the fretting map (Figure 7.4) developed by Vingsbo and Söderberg, it can be seen that the displacements of the 6.5 meter radii bellmouth model, generally falls within in the range of decreasing fatigue life better than the 3 meter radii bellmouth model. This is very speculative since the fretting map is not based on copper, but it still serves as an indication that the 6.5-meter radii model is more prone to fretting fatigue than the 3-meter model.

Table 9: Displacement amplitudes

Location	Bellmouth with radii of 3 m [µm]	Bellmouth with radii of 6.5 m [µm]
Core – Layer 2	39	8
Layer 2 – Layer 3	130	53
Layer3 – Layer 4	190	93
Within Layer 2	33	12
Within Layer 3	64	25
Within Layer 4	68	30

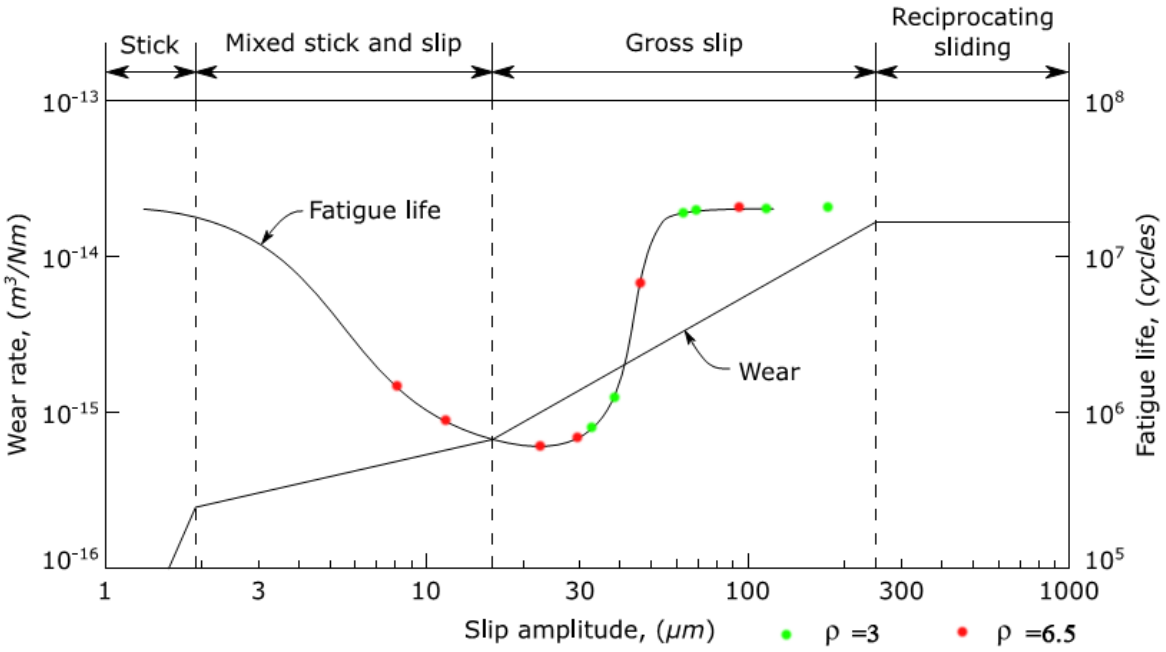

Figure 7.4: Fretting map with displacement amplitudes

The other major parameter governing fretting is the contact pressure. The contact pressure is not explicitly given by the model, and what pressure causing fretting on copper is not found in literature. However, a scatter band of the contact pressure was estimated from the contact line force by division of a lower and upper assumption of a deformed cylinder. The lower assumption was taken as the diameter length and the upper assumption was taken as 10 percent of the diameter. The contact pressure varies as the conductor is being bent. The inline contact pressure fluctuates and reaches zero in the neutral position. The interlayer contacts also fluctuate but remains more or less the same, at maximum the pressure is reduced by 4.6 MPa. The results are shown in Table 10.

Table 10: Estimated contact pressure

Location	Bellmouth with radii of 3 m [MPa]	Bellmouth with radii of 6.5 m [MPa]
Core – Layer 2	4.7 – 47.2	4.9 – 49.8
Layer 2 – Layer 3	2.2 – 22.4	2.19 – 21.9
Layer3 – Layer 4	1- 10.4	0.93- 9.37
Within Layer 2	0.2 – 2	0.089 – 0.89
Within Layer 3	0.53- 5.38	0.23 2.38
Within Layer 4	0.7 - 7	0.3 – 3

No data of contact pressure regarding fretting fatigue of copper was found in literature. However, it was found that an aluminium alloy on steel experience fretting fatigue at 20 MPa and beyond [41]. For stainless steel fretting fatigue is present at 15 MPa [42]. For aluminium fretting fatigue is present at 5 and 20 MPa for two different setups [43].

This data of contact pressure falls within some of the estimated scatter bands of the contact pressures in the conductor. There is a better fit for inter layer contact than for the inline contacts. This suggest that the contact pressure is sufficient to cause fretting fatigue damage also on copper.

8. Discussion

This chapter includes a general discussion and also discussion about mean stress effect and fretting.

8.1 General

All models are an attempt to describe reality, some are useful, and some are not. In this work, a finite element model was developed with the underlying basis that the fatigue life is mainly govern by longitudinal stress ranges. The result shows that the model over predicts the fatigue life when the conductor is subjected to reversed bending in one plane. However, neglecting mean stress correction, the result of the 3-meter radii bellmouth falls within the scatter band of ± two standard deviations from the SN-curve of individual wires. The results from the analytical model are in good agreement with the finite element model prediction.

The predicted life is compared to the laboratory tests, in these tests are all the effects contributing to the fatigue life included by the nature of the test. This comparison (Figure 7.3) suggests that the underlying basis of the model, that the fatigue life is mainly governed by longitudinal stress ranges, may or may not be valid. This depends on whether fretting and the effect of mean stress are present or not.

As already stated, both models overpredicts the fatigue life when comparing to the laboratory tests. However, the amount of overprediction differs between the two models. Assuming the effect of mean stress is negligible, the fatigue life is overestimated by a factor of 1.52 and 9.91 for 3- and 6.5-meters radii bellmouth models, respectively. This means that laboratory tests, especially the longer lives test with the larger radius, fails earlier than what the model predicts. It is normal with large margins in fatigue, and the first factor is indeed predicting life within the scatter band of the SN-curve. Moreover, regarding fretting, the difference of the factors suggests that some fatigue damage comes from fretting.

The influence of the friction coefficient was investigated. It was shown in Table 6 that the predicted fatigue life is very sensitive to the choice of friction coefficient. The coefficient of $\mu = 0.2$ was used and based on the measurement done by Nasution et. al [6]. However, there are some uncertainties regarding this. The friction coefficient may differ from the full-scale tests to the test where the friction coefficient was established. Also, even a change in the second decimal place will affect the predicted life significantly. The friction coefficient may increase during the test as well. Comparing $\mu = 0.2$ to general values of dry copper-copper friction coefficient found in literature, it is quite low.

It was found that the contribution of hoop friction forces was small compare to interlayer friction forces. This servers as a validation of the analytical model that excludes hoop friction forces. The hoop contact elements were removed, this saved computational time but resulted in a higher stress range and thus not considered valid.

The reason for this is assumed to be due to a "hugging" effect increasing interlayer friction force, which comes from the lack of support in the radial direction which the hoop contacts also contributed to.

For the case of the lubricated conductor, there are no final results. However, from the analysis done it can be seen that they are likely not near the scatter band of the SN-curve. It is assumed that the fatigue life of lubricated conductors cannot be explained by friction and therefore not predicted by this model. The fatigue life is governed by other phenomena and perhaps on microscopic level. So, generally low stress ranges do not go well with the model because other phenomena take control over the fatigue life.

8.2 Mean stress effect

There are uncertainties regarding mean stress correction of copper conductors since there have been no research studying this. Dowling stated that the sensitivity of mean stress increases for higher strength metals, since copper has a low strength it is expected to have a low sensitivity. However, for this study, a traditional approach using Goodman correction was used in order to check its influence on the results.

Goodman correction was investigated together with the ultimate strength of copper conductors. A Haig's diagram was constructed by equation 3.5 using the mean stress and the stress range from BFLEX. As can be seen in Figure 7.2 the effects of ultimate strength and Goodman correction is small or for the larger radius possibly even neglectable. The reason for this is that the results from the finite element prediction are close to the R-ratio line of the SN-curve.

Normally, using a lower ultimate strength or a Söderberg relation (same relation as Goodman but with yield stress), adds conservatives. But since the results are both above and beneath the R-ratio line, the mean stress correction is both conservative and unconservative. The predicted life of the 3-meter radii bellmouth model increases and the life of the 6.5-meter model decreases (or stays more or less the same because the results are almost on the R-ratio line). This reduces the difference of the overestimation but moves at the same time the predicted life of the 3-meter radii bellmouth model out of the scatter band. Also, further decreasing the ultimate strength causes an issue as it becomes less than the maximum stress of 226 MPa.

As already stated, the effect of mean stress on copper conductors is not known and the developed model benefits if the sensitivity is low. Since this cannot be concluded in this study, a literature research was done for discussion purposes.

For a study with aluminium, it was found that traditional mean stress sensitivity theory can lead to non-conservative fatigue design [44]. Another study showed, among other things, that the fatigue life on copper is weakly dependent on mean stress [45]. A study on titanium alloy showed that the Goodman relation can lead to significantly over-conservative as well as non-conservative estimations depending on the considered cycles to failure [46]. One study [47] found showed that copper is sensitive to the mean stress effect, but for low stress ranges and relatively low mean stress. However, sensitivity is usually weaker for higher mean stress [48].

So, it is clear that the traditional theories may not be applicable. The sensitivity is dependent on at least what material being used, mean stress and load amplitude, and it seems likely that the sensitivity for copper is low.

8.3 Fretting

The fretting phenomenon is known to be a complex problem to analyse. Little research has been done on fretting related to copper conductors. A literature study was done in order to gain a better understanding of the phenomenon. Even though Nasution et al. found no signs of fretting when investigating fractured wires with a Scanning Electron Microscope, it cannot be ruled out as a possibility. The result of the simulations clearly suggests fretting since the lifetime of the predictions differs significantly. Generally, fretting suffers from the large number of parameters governing the phenomenon, this makes comparisons between studies difficult. Anyhow, contact pressure and displacement amplitude are two parameters that can be used for analysis. With regards to these parameters, the result shows or indicates that fretting is possible. However, these indications of fretting should be taken very briefly as the tribological effects are limited. E.g. the trellis contact is not modelled as a point contact and partial slip phenomenon in fretting is not considered. Also, the contact pressure had to be estimated.

In this study, only the midsection of the conductor and the maximum displacement for each mating surfaces was studied with regards to displacement amplitude and the contact pressure. The displacement amplitude and contact pressure varies from here in location and the contact pressure also varies with time. The contact pressure increases slightly off center and then decreases out to the ends. The interlayer contact force remains sufficiently large over time but the contact within the layers goes to zero when the beam is strait. A more complete analysis would consider all locations in all time steps.

Perhaps the most interesting in this analysis is the displacement and contact pressure between the core and the second layer of the 6.5-meter radii bellmouth model. This fits the reduced fatigue life of Vingsbo's and Söderberg's map well and has likely sufficient pressure to cause fretting fatigue. If this is the case, the fracture also due to fretting would occur in the second layer which is in line with the laboratory tests. The 3-meter radii bellmouth model also shows decreased fatigue life for its displacement amplitude between the core and the second layer. However, since it has a shorter life, it is less exposed to fretting and assumed to be more governed by the stress variation.

As no data on contact pressure on copper was found in literature, data of steel and aluminium was used instead. It is realistic to assume that fretting on copper may occur at the same or even lower levels of contact pressure. The studies found does not investigate a lower threshold for when fretting fatigue is present, which would be of more interest for this study. However, values are taken as the lowest contact pressure when fretting fatigue is present in those studies.

9. Conclusions

The fatigue strength of stranded copper conductors was investigated. A finite element model based on the assumption that fatigue life is mainly governed by longitudinal stress ranges was developed. The predicted life of the model was compared to laboratory tests. The conductor was subjected to static tension and reversed bending in one plane. The main conclusion of this work is that the finite element model overpredicts the fatigue life, by a large factor for the 6.5-meter radius model and by a smaller factor within the scatter band of the SN-curve for the 3.5-meter radius model. The reasons for this are unclear but fretting seems to be a likely explanation. Hence, the model cannot be used for fatigue life prediction of stranded copper conductors. However, some conclusions are drawn from the study.

1. The predicted life is very sensitive to the choice of friction coefficient.

2. The shear stiffness of the contact elements has a significant influence on the predicted life, especially for the 6.5-meter radii bellmouth model.

3. The predicted failure of the unlubricated conductor occurs in the second layer inside the bellmouth. This is in line with the laboratory tests where they occurred in the second or third layer.

4. The analytical model is in good agreement with the finite element model.

5. The contribution of friction forces within a layer is small compare to interlayer friction forces.

6. Traditional use of mean stress correction theory both increases and decreases the predicted life. However, this is uncertain since it is not known how copper conductors respond to the effect of mean stress. A literature study suggests that the sensitivity of mean stress correction is likely low.

7. A simplistic fretting analyses suggest that failure due to fretting damage is most likely to occur in the second layer of the larger radius model.

10. Suggestions for future work

A natural continuation of this work is to further investigate the fretting phenomenon. One can consider performing tests of longer fatigue life in order to capture fretting effects. It is also possible to compare reversed bending tests as done in this work with rotational bending tests. Rotational bending tests should suffer less from fretting because all of the wires are affected. With regards to finite element modelling the next step is to use volume elements, this may or may not improve the results but at a significantly increased computational cost.

No studies where found in literature regarding the mean stress effect of copper conductors. As mentioned in the discussion, the effect of mean stress depends on several parameters and the sensitivity is most likely low. It would therefore be of interest to further investigate and possibly confirm this. This can be done by producing more SN-curves at several different stress amplitudes and R-ratios.

Finally, it is possible to produce SN-curves of whole copper conductors. This would include the possible effects of fretting but makes the SN-curve dependent on the load case.

11. Reference List

1. Council, G.W.E., *Global Wind Report 2018*. 2019.
2. Castro-Santos, L. and V. Diaz-Casas, *Floating Offshore Wind Farms*. 1st ed. 2016 ed. Green Energy and Technology. 2016, Cham: Cham: Springer International Publishing.
3. www.aquaret.com. 2020.
4. Srinil, N., *Cabling to connect offshore wind turbines to onshore facilities*. 2016. 419-440.
5. Worzyk, T., *Submarine Power Cables: Design, Installation, Repair, Environmental Aspects*. Design, Installation, Repair, Environmental Aspects. 2009, Berlin, Heidelberg: Springer Berlin Heidelberg, Berlin, Heidelberg.
6. Nasution, F.P., S. Sævik, and S. Berge, *Experimental and finite element analysis of fatigue strength for 300 mm2 copper power conductor.* Marine Structures, 2014. **39**(C): p. 225-254.
7. Nasution, F.P., et al., *Experimental and finite element analysis of fatigue performance of copper power conductors.(Report).* International Journal of Fatigue, 2013. **47**: p. 244.
8. de Alegría, I.M., et al., *Transmission alternatives for offshore electrical power.* Renewable and Sustainable Energy Reviews, 2009. **13**(5): p. 1027-1038.
9. Thies, P., L. Johanning, and G. Smith, *Assessing mechanical loading regimes and fatigue life of marine power cables in marine energy applications.* Proceedings of the Institution of Mechanical Engineers, 2012. **226**(1): p. 18.
10. DNVGL-ST-0359, *Subsea power cables for wind power plants*.
11. Johnson, K.L., *Contact mechanics*. 1985: CAMBRIDGE UNIVERISTY PRESS.
12. Hobbs, R.E. and K. Ghavani, *The fatigue of structural wire strands.* International Journal of Fatigue, 1982. **4**(2): p. 69-72.
13. Alani, M. and M. Raoof, *Effect of mean axial load on axial fatigue life of spiral strands.* International Journal of Fatigue, 1997. **19**(1): p. 1-11.
14. Hobbs, R.E. and M. Raoof, *Behaviour of cables under dynamic or repeated loading.* Journal of Constructional Steel Research, 1996. **39**(1): p. 31-50.
15. Suh, J.-I. and S.P. Chang, *Experimental study on fatigue behaviour of wire ropes.* International Journal of Fatigue, 2000. **22**(4): p. 339-347.
16. Raoof, M., *Axial Fatigue of Multilayered Strands.* Journal of Engineering Mechanics, 1990. **116**(10): p. 2083-2099.
17. Raoof, M., *AXIAL FATIGUE LIFE PREDICTION OF STRUCTURAL CABLES FROM FIRST PRINCIPLES.* Proceedings of the Institution of Civil Engineers, 1991. **91**(1): p. 19-38.
18. Hobbs, R.E. and M. Raoof, *Mechanism of fretting fatigue in steel cables.* International Journal of Fatigue, 1994. **16**(4): p. 273-280.
19. Karlsen, S., *Fatigue of copper conductors for dynamic subsea power cables*. 2010. p. 275-281.
20. Nasution, F.P., S. Sævik, and J.K.Ø. Gjøsteen, *Fatigue Analysis of Copper Conductor for Offshore Wind Turbines by Experimental and FE Method.* Energy Procedia, 2012. **24**(C): p. 271-280.

21. Nasution, F.P., S. Saevik, and J.K.O. Gjosteen, *Finite element analysis of the fatigue strength of copper power conductors exposed to tension and bending loads.* International Journal of Fatigue, 2014. **59**: p. 114.
22. Kraincanic, I. and E. Kebadze, *Slip initiation and progression in helical armouring layers of unbonded flexible pipes and its effect on pipe bending behaviour.* The Journal of Strain Analysis for Engineering Design, 2001. **36**(3): p. 265-275.
23. *BFLEX Theory Manual*, SINTEF, Editor. 2019.
24. Stig Berge, S.K.Å., *Fatigue and Fracture Design of Marine Structures, Compendium* 2017.
25. Suresh, S., *Fatigue of Materials*. 1998: CAMBRIDGE UNIVERSITY PRESS.
26. Lewinsohn, C.A., *Mechanical Behavior of Materials by Norman E. Dowling*. 2000. p. 775-776.
27. Ralph I. Stephens, A.F., Robert R. Stephens, Henry O. Fuchs, *Metal Fatigue in Engineering*. JOHN WILEY & SONS, INC.
28. D. A.HILLS , D.N., *Mechanics of Fretting Fatigue* ed. G.M.L. GLADWELL. SPRINGER.
29. Björk, K., *Formler och tabeller för mekanisk konstruktion*. Karl Björks Förlag HB.
30. Vingsbo, O. and S. Söderberg, *On fretting maps.* Wear, 1988. **126**(2): p. 131-147.
31. Nowell, D., D. Dini, and D.A. Hills, *Recent developments in the understanding of fretting fatigue.* Engineering Fracture Mechanics, 2006. **73**(2): p. 207-222.
32. *Fretting fatigue: Waterhouse, R.B. Int. Mater. Rev. 1992 37, (2), 77–97.* International Journal of Fatigue, 1993. **15**(4): p. 347-347.
33. Edvardsen, A.V., *Numerical and Experimental Fretting Fatigue Testing Using a New Test Rig*. 2019.
34. Moan, T., *Finite element modelling and analysis of marine structures*. Kompendium (Norges teknisk-naturvitenskapelige universitet. Institutt for marin teknikk). Vol. UK-03-98. 2003, Trondheim: Department of Marine Technology, Norwegian University of Science and Technology.
35. Sævik, S., *Lecture Notes, Advanced Analysis of Marine Structures*
36. Sigmund, O., *Notes and Exercises for the Course: FEM-Heavy.*
37. Ivar Langen, R.S., *Dynamisk Analyse Av konstruktioner*.
38. *RIFLEX Theory Manual*, SINTEF, Editor. 1995.
39. Mathisen, K.M., *Large Displacement Analysis of Flexible and Rigid Systems Considering Displacement-dependent Loads and Nonelinear Constraints*, in *Structural Engineering*. 1990, NTH.
40. Sævik, S.
41. Sadeler, R., *Influence of contact pressure on fretting fatigue behaviour of AA 2014 alloy with dissimilar mating material.* Fatigue & Fracture of Engineering Materials & Structures, 2006. **29**(12): p. 1039-1044.
42. Nakazawa, K., et al., *Effect of contact pressure on fretting fatigue of austenitic stainless steel.* Elsevier Science Publishing Co., Inc., Tribology International (USA), 2003. **36**(2): p. 79-85.
43. Adibnazari, S. and D.W. Hoeppner, *A fretting fatigue normal pressure threshold concept.* Wear, 1993. **160**(1): p. 33-35.
44. Aigner, R., M. Leitner, and M. Stoschka, *On the mean stress sensitivity of cast aluminium considering imperfections.* Materials Science & Engineering A, 2019. **758**: p. 172-184.
45. Eckert, R., C. Laird, and J. Bassani, *Mechanism of fracture produced by fatigue cycling with a positive mean stress in copper.* Materials Science and Engineering, 1987. **91**(C): p. 81-88.

46. Oberwinkler, B., *On the anomalous mean stress sensitivity of Ti-6Al-4V and its consideration in high cycle fatigue lifetime analysis.* International Journal of Fatigue, 2016. **92**(P1): p. 368-381.
47. Lukas, P., et al., *EFFECT OF MEAN STRESS ON THE LOW-AMPLITUDE CYCLIC STRESS-STRAIN CURVE OF POLYCRYSTALLINE COPPER.* Mater. Sci. Eng. A-Struct. Mater. Prop. Microstruct. Process., 1989. **118**: p. L1-L4.
48. Yung-Li Lee, J.P., Richard Hathaway, Mark Barkey *Fatigue Testing and Analysis. Theory and Practice-Butterworth-Heinemann*. 2004: ELSAVIER.

12. Appendix

A) Stress distribution of the conductors in fully bent position.
B) BFLEX input file of the 3-meter radii model.

A)

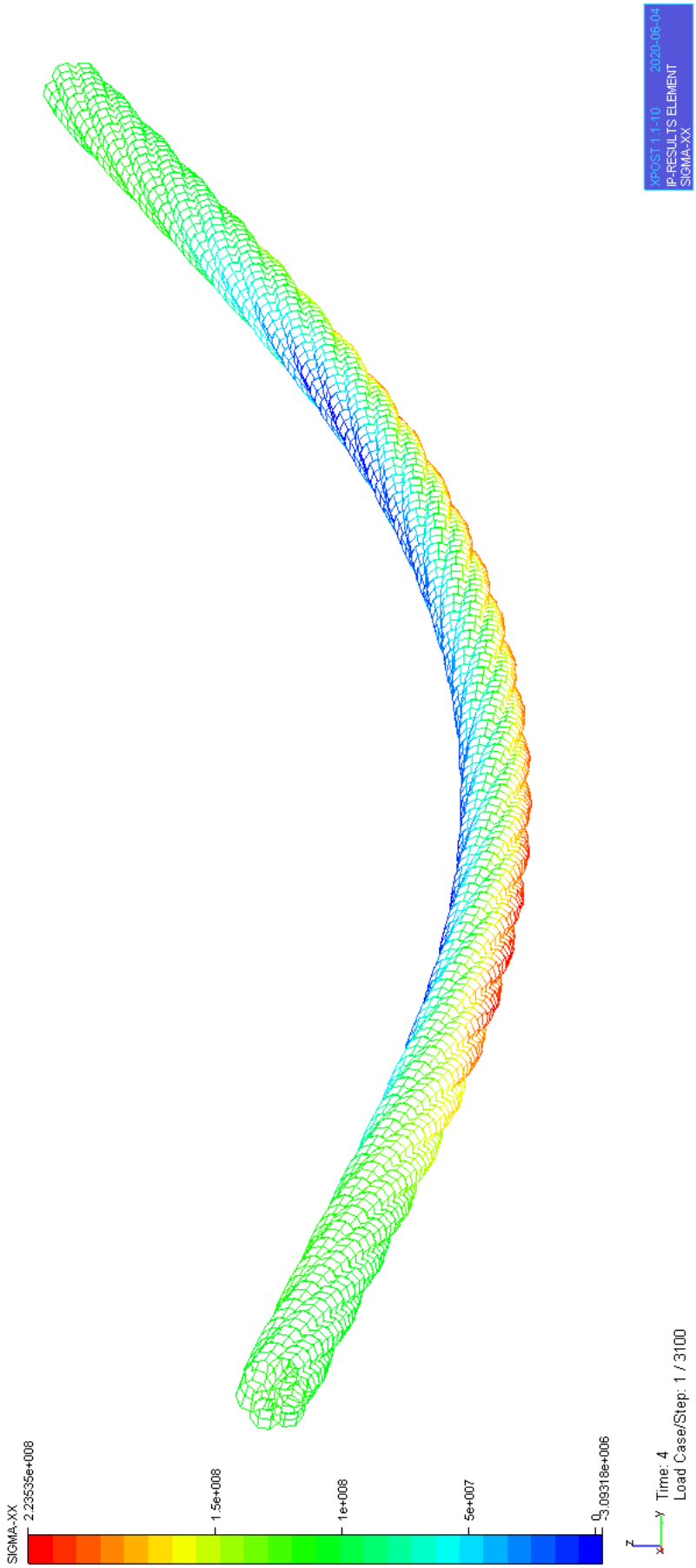

Stress distribution 3-meter radii model att fully bent position.

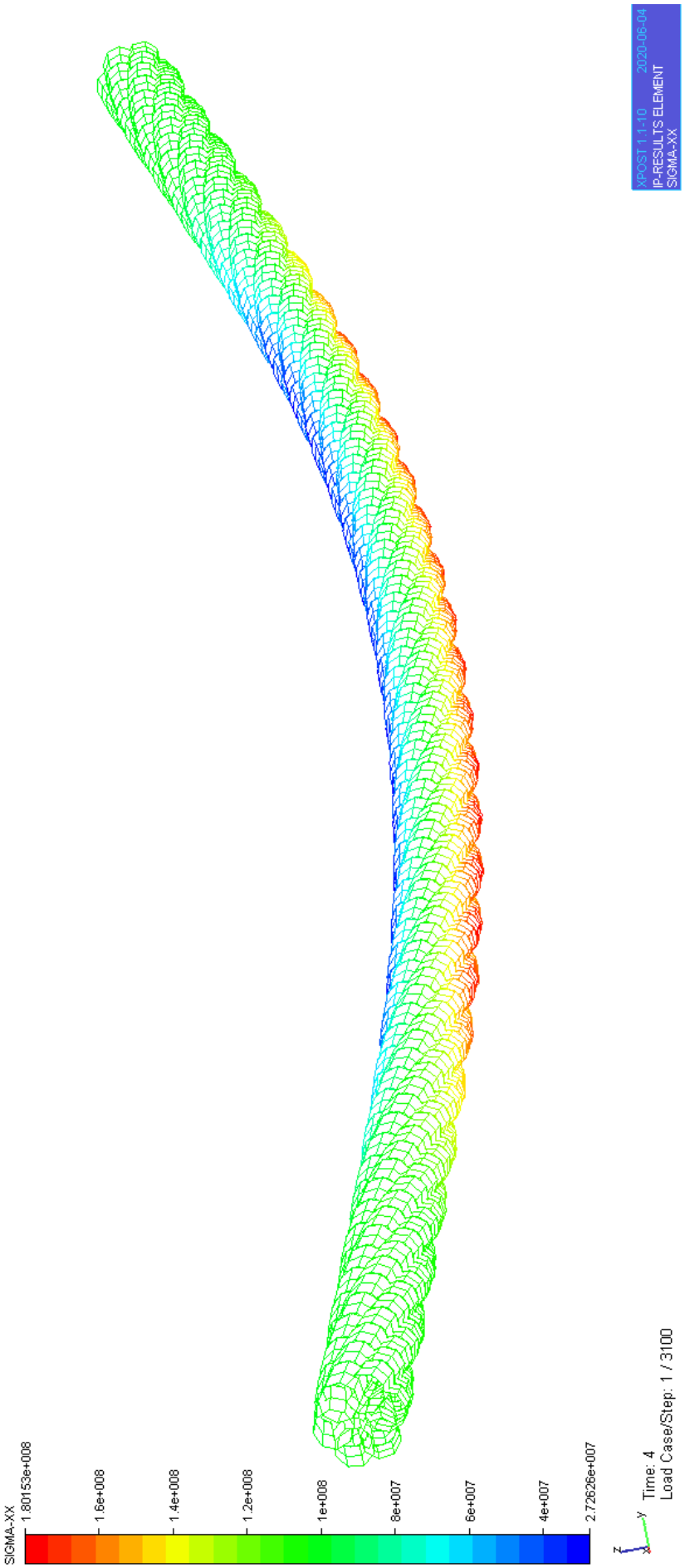

Stress distribution 6.5-meter radii model att fully bent position.

B)


```
1     HEAD M50, BELLMOUTH Length 0.8 RADIUS 3, ELEMENTS = 100 Model Lenght = 1.2 Met
      er
2     HEAD Contact01,
3     HEAD FATIGUE INK.
4     HEAD Units: m, N, Pa, s
5
6     # Control parameters.
7     #       MAXIT   NDIM    ISOLVR  NPOINT  IPRINT  CONR      GAC    ISTRES
8     CONTROL 200     3       2       8       11      10E-05    0   stressfree #  str
      essfree / restart #
9
10    VISRES INTEGRATION      1       SIGMA-XX SIGMA-XX-AX SIGMA-XX-MY SIGMA-XX-MZ V
      CONFOR-Z FATIGUE
11
12    #       MSTAT       ALPHA 1     ALPHA 2     ALPHA
13    DYNCONT  1           0.0         0.05       -0.05
14
15    # Time control data for dynamic iteration
16    #       T       DT    DTVI  DT0    Type    STEPTYPE  ITERCO  ITCRIT  MAXIT  MAX
      DIV  CONR
17    TIMECO  1.0     0.01   0.5  100.0   DYNAMIC  AUTO      NONE    disp     20    1
      0       1.0E-04
18    TIMECO  13.0    0.001  0.5  100.0   DYNAMIC  AUTO      NONE    disp     16    1
      0       1.0E-05
19
20
21    #         NAME   TYPE     POISSON TALFA   TECOND  HEATC BETA  EA          EIY
           EIZ      GIT       EM      GM
22    MATERIAL copper1  LINEAR  0.355   1.1E-5  50      800   0.0   932650      0.59
      936  0.59936  0.442332  1.15E11 0.42435E11
23    MATERIAL copper2  LINEAR  0.355   1.1E-5  50      800   0.0   932650      0.59
      936  0.59936  0.442332  1.15E11 0.42435E11
24    MATERIAL copper3  LINEAR  0.355   1.1E-5  50      800   0.0   932650      0.59
      936  0.59936  0.442332  1.15E11 0.42435E11
25    MATERIAL copper4  LINEAR  0.355   1.1E-5  50      800   0.0   932650      0.59
      936  0.59936  0.442332  1.15E11 0.42435E11
26
27    FATPROP copper1 copperfatigue1
28    FATPROP copper2 copperfatigue2
29    FATPROP copper3 copperfatigue3
30    FATPROP copper4 copperfatigue4
31
32
33    MATERIAL plastic ELASTIC 0.35    1000.0  1.1E-5  0.0   0.0   700E6
34    MATERIAL endmat1 LINEAR  0.35    1.1E-5  50      800   0.0   220640.994  823.6
       823.6 607.8 1.15e11 0.42435E11
35    #
36    #                               TYPE  MUS  MUD  KEL1      KEL2    FRAC  KDYNC1
        C1  C2  DIM   KSURF
37    MATERIAL contact01R2 FRICONTACT  6    0.2  0.2  5159e6    5159e6   2     0.0
        1.0 1.0 -1.0  1e10
38    MATERIAL contact01R3 FRICONTACT  6    0.2  0.2  1298e6    1298e6   2     0.0
        1.0 1.0 -1.0  1e10
39    MATERIAL contact01R4 FRICONTACT  6    0.2  0.2  577e6     577e6    2     0.0
        1.0 1.0 -1.0  1e10
40
41    # The attachecement beams
42    NOCOOR coordinates    5001         0     0    0.00
43                          5011         0     0    0.51
44                          5031         0     0    1.02
45                          #-------Conductor----------#
46                          5032         0.0   0    2.22
47                          5052         0.0   0    2.73
48                          5062         0.0   0    3.24
49    #
50    NOCOOR coordinates    50001        0     0    1.62
51
52
53    #      group      elty       material  ID  n1    n2
54    ELCON  end1      pipe31      endmat1    5001   5001  5002
```

```
55    REPEAT 30 1 1
56    ELCON  end2      pipe31      endmat1    5031   5032  5033
57    REPEAT 30 1 1
58
59    ELORIENT COORDINATES   5001      0.0    1000.0     0.0000
60    REPEAT 60 1 0 0 0
61
62    #      name     type   radius   th      CDr  Cdt  CMr  CMt   wd    ws    ODp
           ODw          rks
63    ELPROP end1     pipe    0.025  0.005    0.8  0.1  2.0  0.2   0.80  0.80  0.012
      5     0.01250     0.5
64    ELPROP end2     pipe    0.025  0.005    0.8  0.1  2.0  0.2   0.80  0.80  0.012
      5     0.01250     0.5
65
66    # BELLMOUTH BODY AND CONTACT.
67
68    ELCON    bellmouth body502 none 90001 50001
69    ELORIENT EULERANGLE  90001   0    0    0
70    ELPROP   bellmouth   body     geo1  0.0  0.0  0.0  0.0  0.0  0.0  0.0  0.0  0.
      0  0.0  0.0  0.0  0.0  0.0 0.0 0.0 0.0 0.0 0.0 0.0
71    #                                      theta   nvis   len      diam   radius
72    GEOM     geo1    1     dTrumpet        0.0     20    0.8     0.030      3.0
73
74    # Contact between bellmouth and conductor
75   ELCON  bscontact cont152 rollmat2  90101  50001
76    REPEAT 101     1     0
77    ELORIENT EULERANGLE  90101   0    0    0
78                         90201   0    0    0
79
80    #        name        type       diameter    inside
81    ELPROP  bscontact bellmouth     0.029     1
82    CONTINT  bscontact    bellmouth  TAPE3    13001     13100      500      500
        0.0    60   1
83
84    #        name           type        mmyx      xname       zname
85    MATERIAL rollmat2       contact     0.2  0.2  rollmat1_x rollmat1_x rollmat1_z

86
87    #        name       type     alfa   eps    sig
88    MATERIAL rollmat1_x epcurve  1      0      0
89                                        0.005  1
90                                        100.00 2
91    #        name          type      eps    sig
92    MATERIAL rollmat1_z    hycurve  -1.0e7 -3.0e15
93                                    1.0e7  3.0e15
94
95    #    BOUNDARY CONDITIONS
96
97    BONCON GLOBAL 5001 1
98    BONCON GLOBAL 5001 2
99    BONCON GLOBAL 5001 3
100   BONCON GLOBAL 5001 4
101
102   BONCON GLOBAL 5062 1
103   BONCON GLOBAL 5062 2
104   BONCON GLOBAL 5062 3
105   BONCON GLOBAL 5062 4
106
107   CONSTR CONEQ global  10001 1 0.0 5031 1 1.0
108   CONSTR CONEQ global  10001 2 0.0 5031 2 1.0
109   CONSTR CONEQ global  10001 3 0.0 5031 3 1.0
110   CONSTR CONEQ global  10001 4 0.0 5031 4 1.0
111   CONSTR CONEQ global  10001 5 0.0 5031 5 1.0
112   CONSTR CONEQ global  10001 6 0.0 5031 6 1.0
113
114   CONSTR CONEQ global  10101 1 0.0 5032 1 1.0
115   CONSTR CONEQ global  10101 2 0.0 5032 2 1.0
116   CONSTR CONEQ global  10101 3 0.0 5032 3 1.0
117   CONSTR CONEQ global  10101 4 0.0 5032 4 1.0
118   CONSTR CONEQ global  10101 5 0.0 5032 5 1.0
119   CONSTR CONEQ global  10101 6 0.0 5032 6 1.0
```

```
120
121   BONCON GLOBAL  50001      1
122   BONCON GLOBAL  50001      2
123   #BONCON GLOBAL  50001      3
124   BONCON GLOBAL  50001      4
125   BONCON GLOBAL  50001      5
126   BONCON GLOBAL  50001      6
127
128   # ROTATION AND SHIFT OF X COORDINATE
129   NOCOOR ROTDISP 0.0  1.57079632  0.0   -1.02 0.0 0.0
130
131
132   # DEFINING NODAL COORDINATES OF CONDUCTOR.
133   # LAYER 1                                                                .
134   NOCOOR COORDINATES   10001    0.0      0.0      0.0
135                        10101    1.20     0.0      0.0
136
137   NOCOOR  COORDINATES  11001    0.00     0.00     0.00
138                        11100    1.20     0.00     0.00
139
140   # TAPES
141   NOCOOR  COORDINATES  12001    0.00     0.00     0.00
142                        12100    1.20     0.00     0.00
143
144   NOCOOR  COORDINATES  13001    0.00     0.00     0.00
145                        13100    1.20     0.00     0.00
146
147   NOCOOR  COORDINATES  14001    0.00     0.00     0.00
148                        14100    1.20     0.00     0.00
149
150
151   # LAYER 2
      .
152   #      no       x0    y0   z0   b1   b2   b3    R          node   xcor  theta
153   NOCOOR Polar  0.0   0.0  0.0  0.0  0.0  0.0    0.00321   200010.00   0
154                                                              20101  1.20   23.7101
      *1.2
155   #           N     NODINC     XINC    THETAINC
156   Repeat      6     101        0.0     6.283185307/6
157
158   # LAYER 3
       .
159   NOCOOR Polar  0.0   0.0  0.0  0.0  0.0  0.0    0.00642   300010.00   0
160                                                              30101  1.20   -22.046
      26*1.2
161   #           N      NODINC     XINC    THETAINC
162   Repeat      12     101        0.0     6.283185307/12
163
164   # LAYER 4
       .
165   NOCOOR Polar  0.0   0.0  0.0  0.0  0.0  0.0    0.00963   400010.00   0
166                                                              40101  1.20   21.2989
      *1.2
167   #           N      NODINC   XINC    THETAINC
168   Repeat      18     101      0.0     6.283185307/18
169
170
171
172   # Defining element groups                                                .
173   # Element connectivity and properties                                    .
174
175   #       ELGR     ELTY        MATNAME      ELID     NOD1    NOD2   NOD3
176   ELCON   LAYER1   HSHEAR363   COPPER1      10001    10001   10002  11001
177   REPEAT  100 1 1
178
179   ELCON   TAPE1    HSHEAR363   PLASTIC      11001    10001   10002  12001
180   REPEAT  100 1 1
181
182   ELCON   TAPE2    HSHEAR363   PLASTIC      12001    10001   10002  13001
183   REPEAT  100 1 1
184
```

```
185   ELCON   TAPE3    HSHEAR363   PLASTIC      13001    10001   10002  14001
186   REPEAT  100 1 1
187
188   #       ELGR     ELTY       MATNAME     ELID   NOD1   NOD2   NOD3   NOD4   .
189   ELCON   LAYER2   HSHEAR353  COPPER2     20001  10001  10002  20001  20002
190                                          20002  10001  10002  20102  20103
191                                          20003  10001  10002  20203  20204
192                                          20004  10001  10002  20304  20305
193                                          20005  10001  10002  20405  20406
194                                          20006  10001  10002  20506  20507
195   REPEAT 100  6 1
196
197   #     ELGR     ELTY          MATNAME     ELID   NOD1   NOD2   NOD3   NOD4
                                     .
198   ELCON LAYER3   HSHEAR353    COPPER3     30001  10001  10002  30001  30002
199                                          30002  10001  10002  30102  30103
200                                          30003  10001  10002  30203  30204
201                                          30004  10001  10002  30304  30305
202                                          30005  10001  10002  30405  30406
203                                          30006  10001  10002  30506  30507
204                                          30007  10001  10002  30607  30608
205                                          30008  10001  10002  30708  30709
206                                          30009  10001  10002  30809  30810
207                                          30010  10001  10002  30910  30911
208                                          30011  10001  10002  31011  31012
209                                          30012  10001  10002  31112  31113
210   REPEAT 100 12 1
211
212   #       ELGR       ELTY     MATNAME     ELID   NOD1   NOD2   NOD3   NOD4   .
213   ELCON LAYER4   HSHEAR353    COPPER4     40001  10001  10002  40001  40002
214                                          40002  10001  10002  40102  40103
215                                          40003  10001  10002  40203  40204
216                                          40004  10001  10002  40304  40305
217                                          40005  10001  10002  40405  40406
218                                          40006  10001  10002  40506  40507
219                                          40007  10001  10002  40607  40608
220                                          40008  10001  10002  40708  40709
221                                          40009  10001  10002  40809  40810
222                                          40010  10001  10002  40910  40911
223                                          40011  10001  10002  41011  41012
224                                          40012  10001  10002  41112  41113
225                                          40013  10001  10002  41213  41214
226                                          40014  10001  10002  41314  41315
227                                          40015  10001  10002  41415  41416
228                                          40016  10001  10002  41516  41517
229                                          40017  10001  10002  41617  41618
230                                          40018  10001  10002  41718  41719
231   REPEAT 100 18 1
232
233   # CONTACT ELEMENTS:
234   #         ELGR          ELTY       MATNAME    ELID     NOD1      NOD2    NOD3
      .
235   ELCON  LAYER1-LAYER2  hcont463   contact01R2  51001    11001     20001   20002
236                                                51002    11001     20102   20103
237                                                51003    11001     20203   20204
238                                                51004    11001     20304   20305
239                                                51005    11001     20405   20406
240                                                51006    11001     20506   20507
241   repeat 100 6 1
242
243   ELCON  LAYER2-TAPE1   hcont463   contact01R2  52001    20001     20002   12001
244                                                52002    20102     20103   12001
245                                                52003    20203     20204   12001
246                                                52004    20304     20305   12001
247                                                52005    20405     20406   12001
248                                                52006    20506     20507   12001
249   repeat 100 6 1
250
251   ELCON  TAPE1-LAYER3   hcont463   contact01R3  53001    12001     30001   30002
252                                                53002    12001     30102   30103
253                                                53003    12001     30203   30204
```

```
                                                    53004    12001     30304   30305
                                                    53005    12001     30405   30406
                                                    53006    12001     30506   30507

                                                    53007    12001     30607   30608
                                                    53008    12001     30708   30709
                                                    53009    12001     30809   30810
                                                    53010    12001     30910   30911
                                                    53011    12001     31011   31012
                                                    53012    12001     31112   31113
  repeat 100 12 1

  ELCON  LAYER3-TAPE2   hcont463   contact01R3    55001    30001     30002   13001
                                                    55002    30102     30103   13001
                                                    55003    30203     30204   13001
                                                    55004    30304     30305   13001
                                                    55005    30405     30406   13001
                                                    55006    30506     30507   13001
                                                    55007    30607     30608   13001
                                                    55008    30708     30709   13001
                                                    55009    30809     30810   13001
                                                    55010    30910     30911   13001
                                                    55011    31011     31012   13001
                                                    55012    31112     31113   13001
  repeat 100 12 1

  ELCON  TAPE2-LAYER4   hcont463   contact01R4    57001    13001     40001   40002
                                                    57002    13001     40102   40103
                                                    57003    13001     40203   40204
                                                    57004    13001     40304   40305
                                                    57005    13001     40405   40406
                                                    57006    13001     40506   40507

                                                    57007    13001     40607   40608
                                                    57008    13001     40708   40709
                                                    57009    13001     40809   40810
                                                    57010    13001     40910   40911
                                                    57011    13001     41011   41012
                                                    57012    13001     41112   41113
                                                    57013    13001     41213   41214
                                                    57014    13001     41314   41315
                                                    57015    13001     41415   41416
                                                    57016    13001     41516   41517
                                                    57017    13001     41617   41618
                                                    57018    13001     41718   41719

  repeat 100 18 1

  ELCON  LAYER4-TAPE3   hcont463   contact01R4    59001    40001     40002   14001
                                                    59002    40102     40103   14001
                                                    59003    40203     40204   14001
                                                    59004    40304     40305   14001
                                                    59005    40405     40406   14001
                                                    59006    40506     40507   14001
                                                    59007    40607     40608   14001
                                                    59008    40708     40709   14001
                                                    59009    40809     40810   14001
                                                    59010    40910     40911   14001
                                                    59011    41011     41012   14001
                                                    59012    41112     41113   14001

                                                    59013    41213     41214   14001
                                                    59014    41314     41315   14001
                                                    59015    41415     41416   14001
                                                    59016    41516     41517   14001
                                                    59017    41617     41618   14001
                                                    59018    41718     41719   14001

  repeat 100 18 1


```

```
320   # INTERNAL LAYER CONTACT ELEMENTS:
                                    .
321
322   ELCON LAYER2IntCont  hcont454    contact01R2  85001    10001     10002   20001
        20002  20102  20103
323                                                 85002    10001     10002   20102
        20103  20203  20204
324                                                 85003    10001     10002   20203
        20204  20304  20305
325                                                 85004    10001     10002   20304
        20305  20405  20406
326                                                 85005    10001     10002   20405
        20406  20506  20507
327                                                 85006    10001     10002   20506
        20507  20001  20002
328   repeat 100 6 1
329
330   ELCON LAYER3IntCont  hcont454    contact01R3  86001    10001     10002   30001
        30002  30102  30103
331                                                 86002    10001     10002   30102
        30103  30203  30204
332                                                 86003    10001     10002   30203
        30204  30304  30305
333                                                 86004    10001     10002   30304
        30305  30405  30406
334                                                 86005    10001     10002   30405
        30406  30506  30507
335                                                 86006    10001     10002   30506
        30507  30607  30608
336                                                 86007    10001     10002   30607
        30608  30708  30709
337                                                 86008    10001     10002   30708
        30709  30809  30810
338                                                 86009    10001     10002   30809
        30810  30910  30911
339                                                 86010    10001     10002   30910
        30911  31011  31012
340                                                 86011    10001     10002   31011
        31012  31112  31113
341                                                 86012    10001     10002   31112
        31113  30001  30002
342   repeat 100 12 1
343
344   ELCON LAYER4IntCont  hcont454    contact01R4  88001    10001     10002   40001
        40002  40102  40103
345                                                 88002    10001     10002   40102
        40103  40203  40204
346                                                 88003    10001     10002   40203
        40204  40304  40305
347                                                 88004    10001     10002   40304
        40305  40405  40406
348                                                 88005    10001     10002   40405
        40406  40506  40507
349                                                 88006    10001     10002   40506
        40507  40607  40608
350                                                 88007    10001     10002   40607
        40608  40708  40709
351                                                 88008    10001     10002   40708
        40709  40809  40810
352                                                 88009    10001     10002   40809
        40810  40910  40911
353                                                 88010    10001     10002   40910
        40911  41011  41012
354                                                 88011    10001     10002   41011
        41012  41112  41113
355                                                 88012    10001     10002   41112
        41113  41213  41214
356                                                 88013    10001     10002   41213
        41214  41314  41315
357                                                 88014    10001     10002   41314
        41315  41415  41416
```

```
358                                                    88015    10001     10002   41415
       41416  41516  41517
359                                                    88016    10001     10002   41516
       41517  41617  41618
360                                                    88017    10001     10002   41617
       41618  41718  41719
361                                                    88018    10001     10002   41718
       41719  40001  40002
362   repeat 100 18 1
363
364
365   #       BOUNDARY CONDTIONS
       .
366   # TAPES
367   BONCON  GLOBAL 11001 2  REPEAT 100 1
368   BONCON  GLOBAL 11001 3  REPEAT 100 1
369
370   BONCON  GLOBAL 12001 2  REPEAT 100 1
371   BONCON  GLOBAL 12001 3  REPEAT 100 1
372
373   BONCON  GLOBAL 13001 2  REPEAT 100 1
374   BONCON  GLOBAL 13001 3  REPEAT 100 1
375
376   BONCON  GLOBAL 14001 2  REPEAT 100 1
377   BONCON  GLOBAL 14001 3  REPEAT 100 1
378
379
380   #LAYERS
381   BONCON  GLOBAL 20001 1  REPEAT 6 101
382   BONCON  GLOBAL 20101 1  REPEAT 6 101
383   BONCON  GLOBAL 20001 2  REPEAT 6 101
384   BONCON  GLOBAL 20101 2  REPEAT 6 101
385   BONCON  GLOBAL 20001 4  REPEAT 606 1
386   BONCON  GLOBAL 20001 5  REPEAT 606 1
387
388   BONCON  GLOBAL 30001 1  REPEAT 12 101
389   BONCON  GLOBAL 30101 1  REPEAT 12 101
390   BONCON  GLOBAL 30001 2  REPEAT 12 101
391   BONCON  GLOBAL 30101 2  REPEAT 12 101
392   BONCON  GLOBAL 30001 4  REPEAT 1212 1
393   BONCON  GLOBAL 30001 5  REPEAT 1212 1
394
395
396   BONCON  GLOBAL 40001 1  REPEAT 18 101
397   BONCON  GLOBAL 40101 1  REPEAT 18 101
398   BONCON  GLOBAL 40001 2  REPEAT 18 101
399   BONCON  GLOBAL 40101 2  REPEAT 18 101
400   BONCON  GLOBAL 40001 4  REPEAT 1818 1
401   BONCON  GLOBAL 40001 5  REPEAT 1818 1
402
403   # Element properties.
404   #       ELGRP      SHEARHELIX      GEOTYPE       W          TH       WD     WS
           SCALEFACT [PHIST GHIST AXISYM]
405   ELPROP  Layer1      shearhelix       tube      0.001605    0.001605   0.1    0.
      1         1      50    50     10
406   ELPROP  Layer2      shearhelix       tube      0.001605    0.001605   0.1    0.
      1         1      50    50     10
407   ELPROP  Layer3      shearhelix       tube      0.001605    0.001605   0.1    0.
      1         1      50    50     10
408   ELPROP  Layer4      shearhelix       tube      0.001605    0.001605   0.1    0.
      1         1      50    50     10
409
410   ELPROP TAPE1        shearhelix       tube      0.004815    0.001605   0.1    0.
      1         1      50    50     10
411   ELPROP TAPE2        shearhelix       tube      0.008025    0.001605   0.1    0.
      1         1      50    50     10
412   ELPROP TAPE3        shearhelix       tube      0.011235    0.001605   0.1    0.
      1         1      50    50     10
413
414   # ELPROP ELGRP         LAYERCONTACT     GAP0   TTIME    CNTR1   CNTR2 SCALEFAC
      T
```

```
415   ELPROP LAYER1-LAYER2   layercontact      D       D       D       0    1.0
416   ELPROP LAYER2-TAPE1    layercontact      D       D       D       0    1.0
417   ELPROP TAPE1-LAYER3    layercontact      D       D       D       0    1.0
418   ELPROP LAYER3-TAPE2    layercontact      D       D       D       0    1.0
419   ELPROP TAPE2-LAYER4    layercontact      D       D       D       0    1.0
420   ELPROP LAYER4-TAPE3    layercontact      D       D       D       0    1.0
421
422   ELPROP LAYER2IntCont   layercontact      D       D       D       0    1.0
423   ELPROP LAYER3IntCont   layercontact      D       D       D       0    1.0
424   ELPROP LAYER4IntCont   layercontact      D       D       D       0    1.0
425
426   # Contacts
427   CONTINT LAYER1-LAYER2     LAYER1   LAYER2   1      3      0.0      0.0     0
         60    2
428   CONTINT LAYER2-TAPE1      LAYER2   TAPE1    1      3      0.0      0.0     0
         60    2
429   CONTINT TAPE1-LAYER3      TAPE1    LAYER3   1      3      0.0      0.0     0
         60    2
430   CONTINT LAYER3-TAPE2      LAYER3   TAPE2    1      3      0.0      0.0     0
         60    2
431   CONTINT TAPE2-LAYER4      TAPE2    LAYER4   1      3      0.0      0.0     0
         60    2
432   CONTINT LAYER4-TAPE3      LAYER4   TAPE3    1      3      0.0      0.0     0
         60    2
433
434   CONTINT LAYER2IntCont     LAYER2   LAYER2   1      3      0.0      0.0     0
         60    2
435   CONTINT LAYER3IntCont     LAYER3   LAYER3   1      3      0.0      0.0     0
         60    2
436   CONTINT LAYER4IntCont     LAYER4   LAYER4   1      3      0.0      0.0     0
         60    2
437
438
439
440   # ELEMENT ORIENTATION.
441   #            TYPE          ElementID    X      Y    Z
442
443   ELORIENT COORDINATES       10001        0.0   1.0  0.0
444                              10100        0.0   1.0  0.0
445
446   ELORIENT COORDINATES       11001        0.0   1.0  0.0
447                              11100        0.0   1.0  0.0
448
449   ELORIENT COORDINATES       12001        0.0   1.0  0.0
450                              12100        0.0   1.0  0.0
451
452   ELORIENT COORDINATES       13001        0.0   1.0  0.0
453                              13100        0.0   1.0  0.0
454
455
456   ELORIENT COORDINATES       20001        0.0   1.0  0.0
457                              20600        0.0   1.0  0.0
458
459   ELORIENT COORDINATES       30001        0.0   1.0  0.0
460                              31200        0.0   1.0  0.0
461
462   ELORIENT COORDINATES       40001        0.0   1.0  0.0
463                              41800        0.0   1.0  0.0
464
465   ELORIENT COORDINATES       85001        0.0   1.0  0.0
466                              85600        0.0   1.0  0.0
467
468   ELORIENT COORDINATES       86001        0.0   1.0  0.0
469                              87200        0.0   1.0  0.0
470
471   ELORIENT COORDINATES       88001        0.0   1.0  0.0
472                              89800        0.0   1.0  0.0
473
474
475   #        TYPE            ElementID   X     Y       Z
476   ELORIENT eulerangle      51001       0.0   0.0     0.0
```

```
                            51600       0.0   0.0     0.0

  ELORIENT eulerangle       52001       0.0   0.0     0.0
                            52600       0.0   0.0     0.0

  ELORIENT eulerangle       53001       0.0   0.0     0.0
                            54200       0.0   0.0     0.0

  ELORIENT eulerangle       55001       0.0   0.0     0.0
                            56200       0.0   0.0     0.0

  ELORIENT eulerangle       57001       0.0   0.0     0.0
                            58800       0.0   0.0     0.0

  ELORIENT eulerangle       59001       0.0   0.0     0.0
                            60800       0.0   0.0     0.0

  # External pressure and gravity(=0).
  PELOAD  50 50
  THIST   50
          0.0  1.0
          1.0  1.0
          13.0 1.0


  # Tensile load as strain.
  INISTR  110    1   5001  0.135967   5060   0.135967
  THIST   110    0  0.0
                 0.1  0.001
                 1  1.0
                10  1.0
               360  1.0


  # Movement of bellmouth
  CONSTR PDISP  GLOBAL 50001  3 -0.18 300
  THIST_R 300   1.0 4.0 rampcos  1.0
                4.0 7.0 rampcos -1.0
                7.0 10.0 rampcos 1.0
                10.0 13.0 rampcos -1.00
```

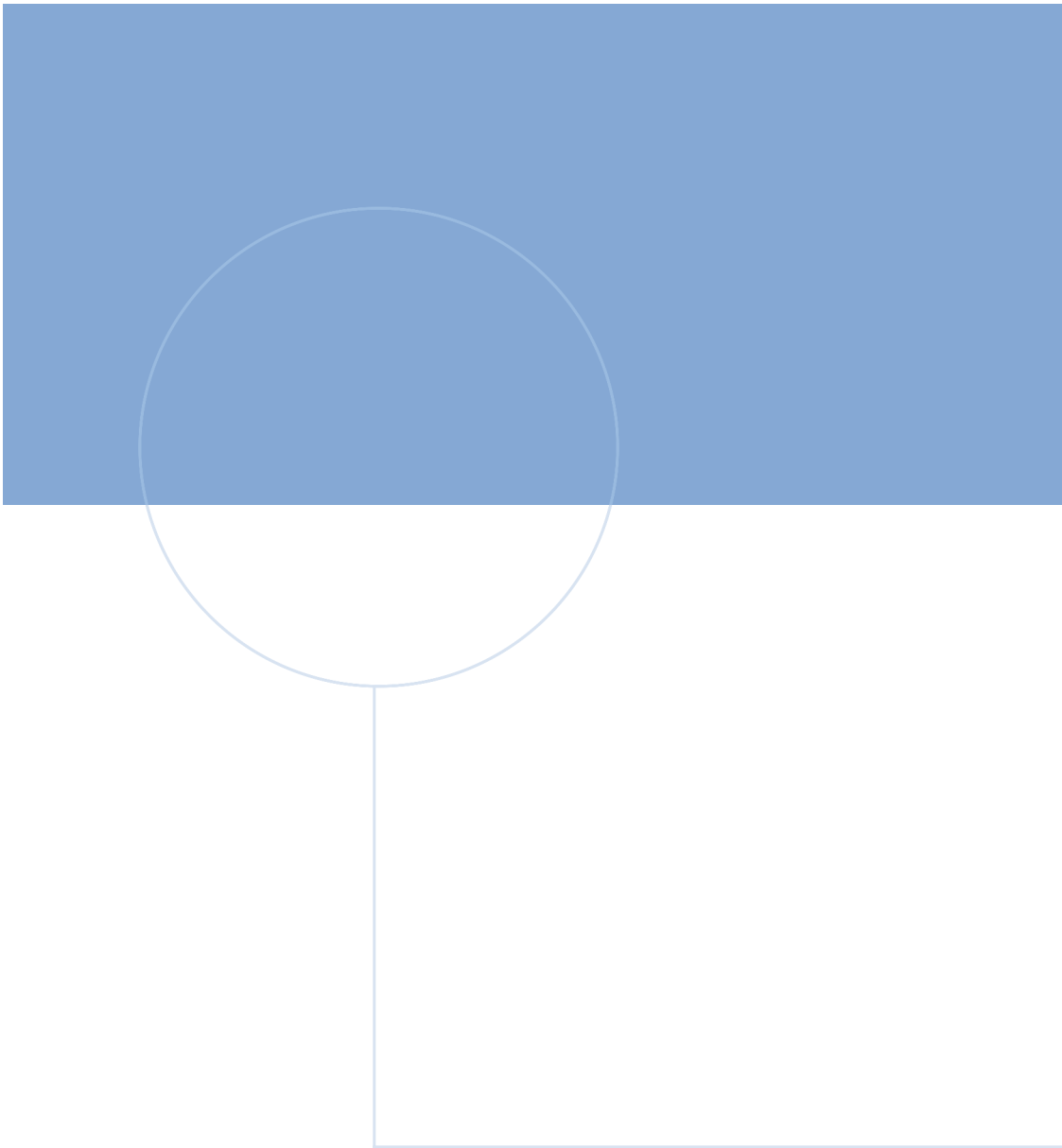

NTNU

Norwegian University of
Science and Technology